Femtosecond laser pulses interacting with atoms: High-order Harmonic Generation

By

Moses Eshovo Ojo[1]

Thesis Supervisor: Prof. Anatole Kenfack

A thesis submitted in fulfillment of the requirements for ***Masters Degree in Theoretical and Applied Physics***

African University of Science and Technology [AUST], Km 10 Airport Road, F.C.T Abuja, Nigeria
www.aust.edu.ng

September 16, 2019

[1]email:mojo@aust.edu.ng

Femtosecond laser pulses interacting with atoms: High-order Harmonic Generation

By

Moses Eshovo Ojo

A THESIS APPROVED BY THE DEPARTMENT OF THEORETICAL AND APPLIED PHYSICS

I, the undersigned, hereby declare that the work contained in this thesis is my original work, and that any work done by others or by myself previously has been acknowledged and referenced accordingly

.....
Moses Eshovo Ojo
(Student Name)

.....
Prof. Anatole Kenfack
(Thesis Supervisor)

.....
Prof. Anatole Kenfack
(Head, Department of Theoretical and Applied Physics)

.....
Prof. Charles Chidume
(Vice President Academic)

.....
Date

The final copy of this thesis has been examined by the signatories, and we find that both the content and the form meet acceptable presentation standards of scholarly work in the above mentioned discipline.

ABSTRACT

We theoretically investigated a phenomena arising from the interaction of femtosecond pulsed lasers with an Hydrogen atom. The phenomena of interest to us, is the High order Harmonic Generation (HHG) of soft and hard-Xray using linearly polarized two-color femtosecond laser pulses. This HHG process is a commonly employed technique to produce ultrashort intense light spanning through the ultraviolet to the x-ray region of the Electromagnetic Spectrum (EM). The development of HHG which has opened fascinating research at sub- atomistic scale is however been delimited by its lower higher-order harmonics, and the possibility of obtaining a single burst of attosecond (which is of high important, since significant amount of the laser energy are carried by single pulses) are been compromised. We began addressing this challenge, by solving the 1D non-relativistic Schrödinger equation for an H atom using the dipole approximation, whose solution was obtained by the split operator method. We separately computed the HHG spectrum due to a Titanium-Sapphire (fundamental field) and an arbitrary pulsed laser (secondary field) in the far-visible region. When the fundamental Ti:Sapphire laser field with the parameters; 800 nm, $2{\times}10^{14}W/cm^2$ and 10 cycles, were allowed to irradiate the H atom, we observed a train of 1330 as pulses extending from the 8^{th} - 36^{th} harmonic order, and whose energy measured 12 eV -55.8 eV. By considering the interaction of a similar Ti:Sapphire laser, with a different intensity of $4{\times}10^{14}W/cm^2$, we observed a train of 677 as pulses extending from the 25^{th} - 75^{th} harmonic order and whose energy measured 39 eV - 116 eV. When the secondary laser source in the far visible region with the parameters; 400 nm, $5{\times}10^{14}W/cm^2$ and 20 cycles irradiated the H atom, a train of 1209 as pulses extending from the 28^{th} - 50^{th} harmonic order, and whose energy corresponds to 87 eV - 155 eV was generated. Furthermore, by synthesizing the fundamental and secondary laser, and upon irradiation with the H atom, an HHG spectrum with a broad plateau whose energy spans through the ultraviolet region up to the hard X-ray region was observed. The broadness of the plateau implies the generation of short pulses, which also represents a clear indication of the possibility of obtaining a single attoseconds pulse. Though by considering a time delay in the synthesized laser there weren't obvious change of our results, we finally obtained a continuum of an abrupt end at the 685^{th} order corresponding to a single pulse of 1.044 keV of energy with a short time duration of 169 as.

Keywords: Attosecond pulses, femtosecond pulses, High order Harmonic Generation, laser fields, spectrum, H atom.

ACKNOWLEDGEMENT

I appreciate God's love on me. My warm kudos goes to my supervisor, Prof. Anatole Kenfack. His effort toward the completion of this work is not quantifiable. I think its a privileged and honour to behave such such a sound and intelligent supervisor like you. It was an excellent supervision from him. He made me realize that though research isn't easy, but with a sound understanding of *the very fundamentals* coupled with persistent strive one can achieve breakthrough. He is always and at all time readily available for any discussion when this work lasted. I will now and always appreciate your research experience and patience-for the both have indeed made this work a huge success. You made me believe in myself, that ;I can do it. Now I can confidently say that I have been well groomed and ready to launch out into the global research community.

And to everyone at AUST including the Board of Governors, Hod's, Faculties, staff, students and especially to all my lecturers who had travelled down to Nigeria. I appreciate you all, for it has been a nice time having you all around. I will not forget to appreciate my family. Thank you so much for your prayers and good wishes. It wouldn't have been easy if I hadn't had them. I love you so much.

DEDICATION

I dedicate this work to my late dad, mum, siblings and Gift. You are the best family to have. Love you all.

CONTENTS

LIST OF TABLES

LIST OF FIGURES

INTRODUCTION

Over the years, the need to probe into smaller dimensions became necessary. Activities happening in very small time scales have successfully been exploited using lasers [1]. Lasers are ultra fast and strong electromagnetic field with time duration in the order of $10^{-15}s$ and $10^{-18}s$. These ultra fast light are employed to probe into processes occurring within atoms and molecules [2]. Lasers have found wide applications in the areas of inhibiting cancerous cells growth, coherent diffractive imaging in microscope, tracing chemical reaction, monitoring/control of electron dynamics in atoms to mention a few [3].

Our main interest of laser application will be limited to research purposes, where lasers have been employed to follow ultra fast inner shell electron dynamics. Lasers with time scale of the order of $10^{-18}s$ otherwise reffered to as attoseconds lasers are used to investigate these phenomena which occur in time scales shorter than 1 femtosecond[3]. Quite a number of techniques have been devised to produce attoseconds lasers, to include spontaneous emission from free electron lasers, Thompson scattering process and High-order Harmonic Generation(HHG) from gaseous and solid surfaces [3]. So far, HHG is the most promising way to produce attosecond extreme ultraviolet pulses, owing to the use of moderate intensity of incident light pulses compared to other technigues [4]. HHG occurs when a moderate intense femtosecond laser field interacts with an atomic gas target in such a way as to cause suppression of the soft-core arms of the gases. The gas medium responds in a highly non-linear way by generating radiation with higher frequencies co-propagating with the fundamental laser beam. The resulting spectra will consist of odd multiples of the the fundamental frequency [3].

The HHG process predominantlly gives rise to the production of train of attosecond pulses. However, the interest of researchers are in the production of a single burst of attoseconds rather than a train of pulses, and this has been realisesd via temporal gating, spatial gating and spatio-temporal gating. The HHG process is well understood from the 3 step semiclassical model developed by Lewestein et al. for linearly polarized field, and which was later extended by Milosevec to include elliptically polarized field [4, 5]. Under the 3-step model, electrons ionizes from the (ground state) coulombic atomic attraction by tunneling, onces in the continuum, the laser field propagates the electron forth and back, thereby making several collisons with the atomic core, with the result that high intense and ultrashort pulses are generated. These pulses have energies in the extreme and X-ray region. The ability of the HHG process to convert light of a given wavelength into extreme ultraviolet/x-ray light (which is of lower wavelenght) is measured by it conversion efficiency. Recent research have been geared towards improving the non-linear conversion efficiency of the HHG process to make this process favourable over other pathways leading to attosecond pulse generation [6].

By interacting a single laser beam with the gas system, attoseconds pulses of energies within the extreme ultraviolet region of the EM spectrum have been generated. However, inorder to extend the pulses energy beyong the extreme ultraviloet region into the hard X-ray, researchers have done several works by superimposing two distinct laser beam(different frequencies/colours) on a gas system. It is also worth noting that the optimization of this two color mixing technique have been achieved through time delay,

intensity variation and phase difference between the interating laser sources. This optimization technique has resulted to the generation of short time duration pulses of 100-200 as [6, 7, 8, 9].

Our aim in this research is to explore and implement a handful of the two colour technique mixing of incident femtosecond lasers (800 nm), with a 400 nm femtosecond lasers, which to the best of our knowledge, has not yet been utilized. Both laser sources, Titanium-Sapphire (800 nm) and 400 nm laser have been successfully generated experimentally[10].

This work have been systematically arranged into five chapters. Chapter one focuses on the basic fundamentals of lasers. The Chapter discusses the principles of femtosecond laser generation, properties of lasers and their mathematical representation. Chapter two is centered on HHG process. It describes the manner in which the femtosecond lasers in Chapter one, are used to generate attosecond pulses through the HHG process. Three commonly used approaches for explaining the HHG process was examined namely; The Simple Man's Model, Strong Field Approximation Model and Direct integration of the TDSE. While Chapter three examines a number of the techniques that have been employed to isolate a single attosecond pulse from a train of pulses. Chapter four outlines the algorithm of the computational simulations involved in the work. It specifies explicitly, the defination of all terms (grid boundary, absorber potential, soft-core potential, wavefunction and energy) used in the simulation. The results of the work are then presented in Chapter five. The discussion of the results and their implications in research have been outlined. Throughout this work atomic units ($a.u$) are considered (see Appendix A), unless otherwise stated.

CHAPTER 1

FUNDAMENTALS OF LASER

1.1 Basics of Light

Light is a form of energy that provides a visual aid to the human eye. Light enables one to take full cognisance of his immediate environment. The extent to which a particular light source can probe into a given surrounding depends on the intensity of such light. So, light of higher intensity can be more informative than an ordinary light, owing to their power of greater penetration (high frequency). The Electromagnetic Spectrum of Figure 1.1 characterizes all forms of light. The frequency increases from left to right, while wavelength decreases. Typically used femtosecond lasers for HHG processes fall within the near-Infrared region, while the resulting attosecond pulse, have energies ranging from the ultraviolet - X ray light region. The radio and micro waves found at the extreme left of the spectrum are lowest in frequency(energy) but highest in wavelength. The high intensity components of the spectrum are those located to the extreme right of the spectrum, which are capable of exploring detailed information about matter [2].

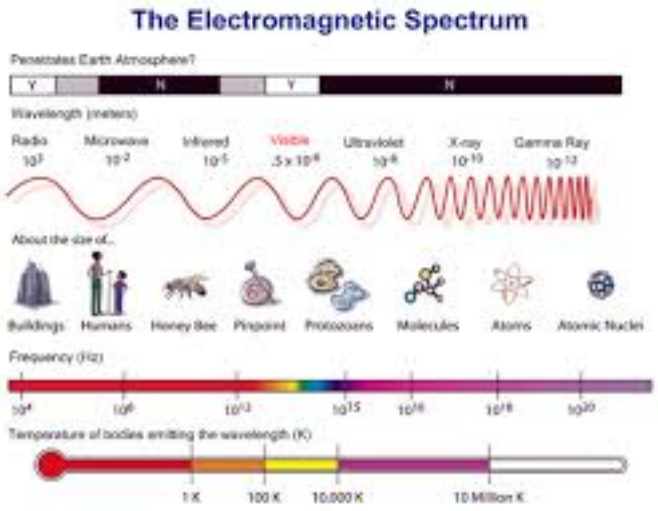

Figure 1.1: The Electromagnetic (EM) Spectrum [17]

.

All natural and artificial light sources can be classified under one of the components in the spectrum. Solar radiation from the sun has varying proportion of the spectrum components as shown in Figure 1.2. Majority of the components goes undetected by the human eye, and only a little portion of the radiation (spanning the visible light region) are visible to the eye. Though, the other parts of the spectrum remains invisible to the human eyes, but their effects can be felt. [18].

Each component in the spectrum consists of a magnetic and electric field component, vibrating at an orientation of right angles to one another. As a common property, to

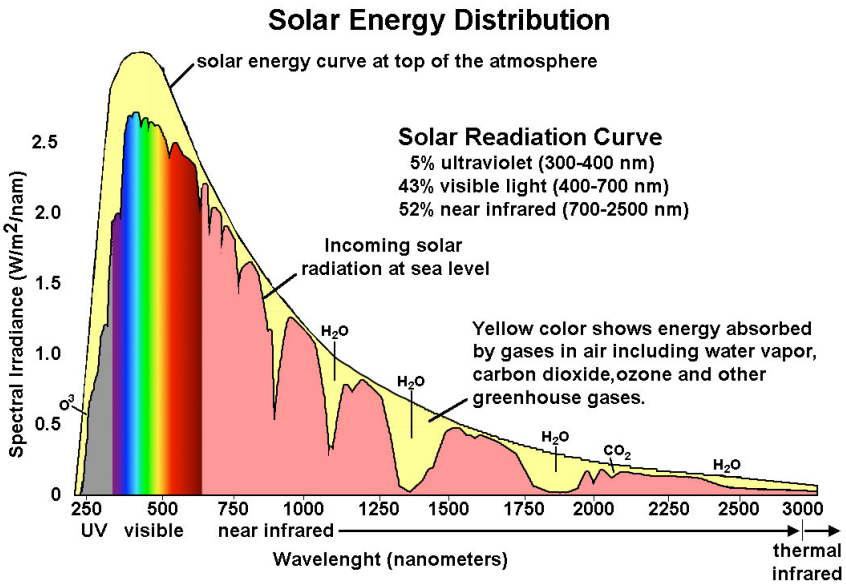

Figure 1.2: Solar Spectrum: 80 percent of the spectrum is occupied by the visible region [19].

all components, they travel at the speed of light [18]. Laser is however a special light with some unique properties. Laser light are emitted coherently in space and time. The photons that makes up laser light are emitted exactly in phase to each other [15]. So that, their intensities add up, and a narrow light is observed. It will be no mistake to say that laser light (or simply laser) are 'super light'. Table 1.1 below displays the difference between an ordinary light and a laser.

Table 1.1: Difference between ordinary and laser light

Properties	**Ordinary light**	**Laser light**
Frequency	multiple color	monochromatic
Pattern of travel	diffuse	highly directional
Beam size	broad beam diameter	pencil-like beam
Intensity and power(within an EM region)	moderate	high

1.2 Principle of Femtosecond Lasers Generation

Ordinary light (or simply light) is the starting point for laser generation. When light interacts with matter (a gaseous medium) a repeated sequence of excitation and de-excitation occurs to produce typically femtoseconds laser [15]. These processes can be summarized under the following headings;

(a) Absorption of incident photon

(b) Stimulated emission of electrons

(c) De-excitation of irradiated atom (/Spontaneous emission of light)

Consider a 2-level system of atoms, which are initially in the ground state. By 2-level, we mean that the system can exist in two (2) discrete energy state (a lower and a higher excited state). When light of energy equal to the energy difference between the levels is incident on the system, the electrons upon absorbing the energy makes a transition to the excited state. This results to a decrease in the population level of atoms in level 1 (ground state), and a subsequent increase in level 2 (excited state). The relationship between the population of any two level system at thermal equilibrium is given by the Boltzmann principle (a fundamental law of thermodynamics);

$$N_2 = N_1 e^{-}\left(\frac{E_2 - E_1}{kT}\right) = N_1 e^{-}(\frac{h\upsilon}{kT}) \tag{1.1}$$

where N_2 and N_1 are the population of the upper and lower states, respectively, E_2 and E_1 are energies corresponding to the upper and lower states respectively, T the equilibrium temperature, and k the Boltzmann constant, h the Planck's constant and υ the frequency of light. For a normal population of the atoms, there will always be more atoms in the lower energy state than in the upper ones. In order to achieve stability after excitation, the electrons in the excited state will decay to their ground state after the elapse of a characteristic time defining the time constant of level 2. When such a decay occurs without the influence of an external field, several photons will be emitted in random directions, in a process called *spontaneous emission*. However, these stochastic emission of photons and the the poorly populated higher energy state are detrimental to the production of lasers. Achieving a relatively high number of atoms in the excited state requires an induced process called *population inversion*. While the naturally decay of electrons to a lower state can be inhibited, so that stimulated decay occurs with the influence of an external field, a continous stream of laser production can be sustained [18] as seen in Figure 1.3.

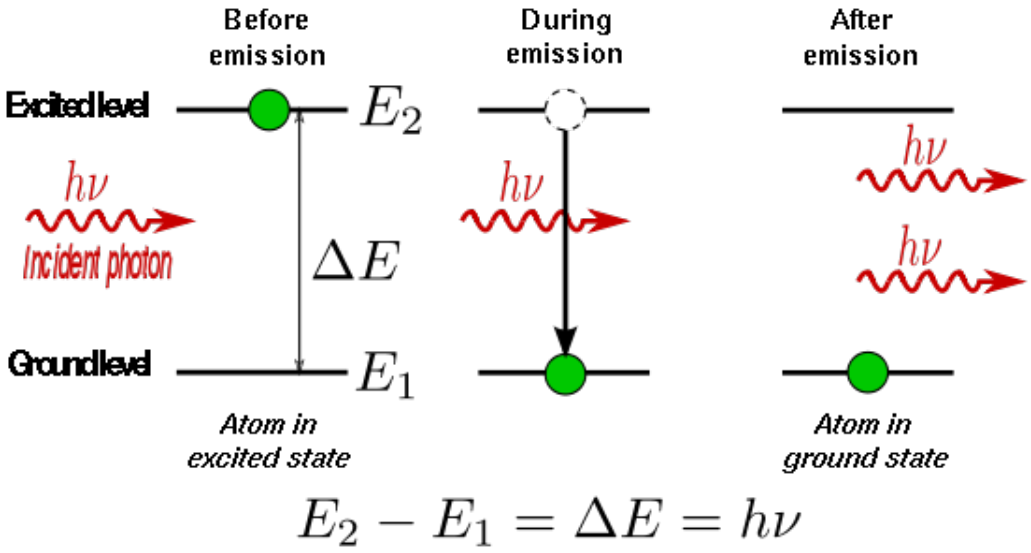

Figure 1.3: A 2-level atomic system[24].

In practice, stimulated decay cannot be achieved with a two (2) level atomic system. This is due to the fact that the decay life of the excited state are usually very short, so that the electrons return to their ground state soon after been excited. Therefore, the possibility of allowing an external field to initiate the decay may not be achieved. The 3 -level atomic system is a realistic system for laser production. It was used to produce the first type of laser; *ruby laser* in 1960. The 3 -level system is rather ineffiecient because of the strong pumping action required to achieve population inversion. But a 4 -level atomic system is sufficient to achieve stimulated emission, and also population inversion.

The design of the 4 -level system allows majority of the excited atom to remain in some intermediate state (level 3) for a longer time before decaying to another state (level 2), and finally to the ground state. During their stay in level 3, an external photon of energy equal to the energy difference between level 3 and level 2 will stimulate the atoms to return to level 2. This process is accompanied by the release of a photon having the same wavelength, in exactly the same direction and in phase as the stimulating photon. The *emitted photon* and the *stimulating photon* couples together to form **laser light** with higher intensity and spatial/temporal coherence. Thus spontaneous emission resulting to incoherent radiation is avoided. By considering a linear assembly of atoms, the intensity of the generated laser can be progressively increased by allowing the coupled light from a previous atom to interact with the next atom in space. The coupled light generated at each atomic site, would serves as the stimulating photon for the next atoms. The next atom gets excited and undergoes relaxation to level 2 and subsequently to the ground state. The de-excitation process will be accompanied by the release of another coupled light, this new coupled light now couples with the previous one,to produce a 4-coupled light, with a much higher intensity. These sequential amplification of the laser occurs all along the assembly of the atoms [18].

In a typical laser set-up as seen in Figure 1.4, there is usually a mirror system used to reflect the generated photons (laser), so that they can have the opportunity to interact with the atom several times, thereby sustaining the process. Though, spontaneous emission of the excited atoms occus but to a lesser degree, and since their emissions result to fluorescence and do not contribute to laser generation, they are reflected out of the system [15].

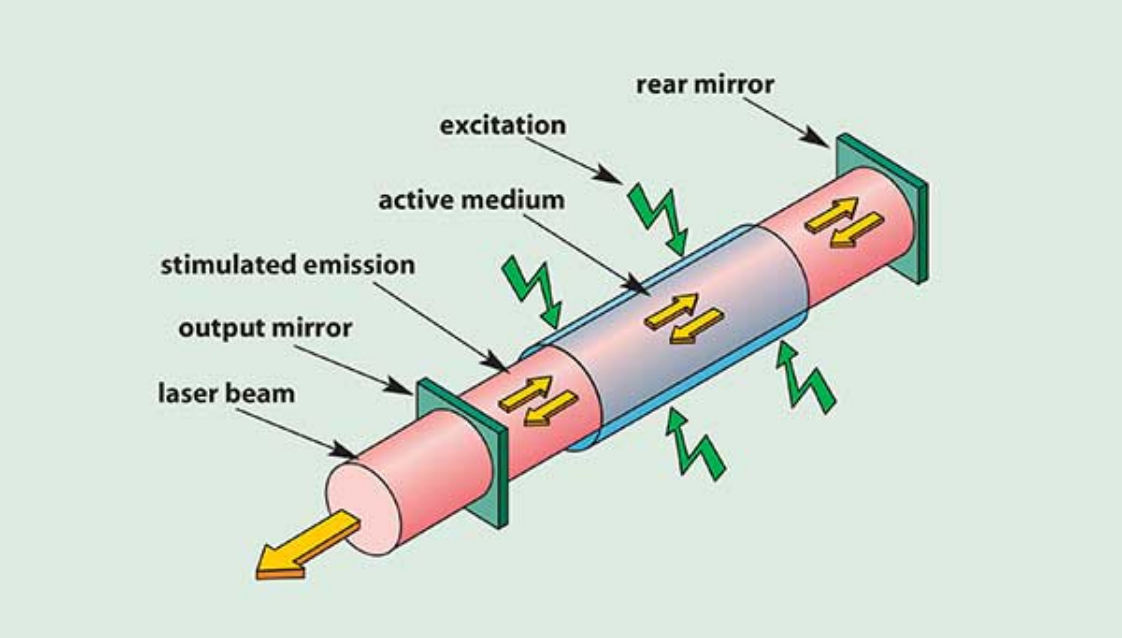

Figure 1.4: Principle of femtosecond laser generation[3].

There are quite a number of mechanism employed to achieve population inversion. Optical pumping, electrical pumping and chemical pumping are among techniques employed. This involves pumping the active medium (gas target-noble gases)in order to excite the atoms. The atomic density in the metastable population level concerned with population inversion and subsequently laser generation is given by [15];

$$\frac{dN_2}{dt} = W_{03}N_0 + W_{13}N_1 - (A_{21} + \ A_{20})N_2 = 0 \tag{1.2}$$

$$\frac{dN_1}{dt} = w_{01}N_0 + (W_{13} + w_{10})N_1 \ + A_{21}N_2 = 0 \tag{1.3}$$

$$N_o + N_1 + N_2 + N_3 = N \tag{1.4}$$

where N_o, N_1, N_2, N_3 are the respective level population. N is the total number of atoms in the active medium, A_{21} and A_{20} are the Einstein coefficient characterizing transition from $2 \rightarrow 1$ and $2 \rightarrow 0$, respectively. w_{01} and w_{10} are thermal transition probabilities for transition $0 \rightarrow 1$ and $1 \rightarrow 0$ respectively, W_{03} and W_{13} are induced transition probability per unit time for transition $0 \rightarrow 3$ and $1 \rightarrow 3$ respectively, caused by the stimulating radiation.

1.3 Characterization of Lasers

The energy of a laser beam usually extends from micro wave region far into the X-ray region. The wavelength of the incident light needed for laser genration determines the wavelength of the resultant intensified light (laser). Table 1.2 below depicts a list of common lasers. The laser type are named according to the gas target medium used in their generation. Broadly speaking lasers can be described as been solid state lasers (e.g Neodymium :YAG laser), gaseous lasers (CO lasers, CO_2 laser, Helium-Neon laser), dye lasers or semiconductor lasers . Solid state lasers are produced from a solid active medium, while gaseous lasers are generated from gaseous target, and dye lasers have as their active medium as a complex organic dye in liquid solution [23].

Table 1.2: Common types of lasers

	Laser type	**Wavelength** (nm)
(i)	Free electron	UV- X ray
(ii)	Excimer : Argon Flouride	193
(iii)	Nitrogen	337
(iv)	Argon ion (blue)	488
(v)	Argon ion (green)	514
(vi)	Helium Neon (blue)	633
(vii)	Ruby ($CrAlO_3$)	694
(viii)	Rhodamine 6G Dye (tunable)	570 - 650
(ix)	Ti:Sapphire	650 - 1100
(x)	Nd:YAG	1064
(xi)	Carbon dioxide	1064

A few types of lasers like, Ti:Sapphire lasers, Ytterbium laser and Free Electron Laser shall be investigated.

- Ti:Sapphire lasers: Ti:Sapphire refers to a crystal of Sapphire (Al_2O_3) that is doped with Titanium ions. Ti:Sapphire which acts as the active medium in the production of Ti:Sapphire lasers are usually pumped with argon ion lasers (514 nm). Having a broad wavelength range from 650nm to 1100 nm, these lasers are mainly used

in scientific research because of their ability to generate ultrafast lasers, and their tunability [23]. In this work we shall make use of this laser type as our fundamental laser.

- Nd:YAG Laser: Neodynium Ytterbium (Nd:YAG) lasers are solid state lasers in which Nd:YAG is the active medium. Nd:YAG laser generates laser light commonlly in the near infra red region of the spectrum at 1064 nm. They also emit laser light at several differnt wavelenght of 1440 nm, 1320 nm, 1120 nm and 940 nm. Optical pumping of Nd:YAG with laser diode is done to excite the Nd ions to an excited state, upon which an external photon will act to cause stimulated emission [15].

- Free Electron Laser (FEL): The active medium of a Free Electron Laser consist of very high speed electrons moving freely through a magnetic structure called an undulator. The undulator generates a periodically varying Lorentz force, which forces the electrons to radiate with a certain range of frequencies, ranging from microwaves through terahertz radiation and infra red to the visible spectrum, ultraviolet and X-ray. As such, they are tunable lasers. They occupy a huge position in the heart of researchers as they are heavily sought for. The only draw back of FEL is that, their set up are very large and expensive, so that they can only be used at relatively few large facilities in the world. An infrared FEL has been built in Dresden (Rossendorf) and the FEL (formerly VUV-FEL)at DESY in Hamburg generates radiation in the soft X-ray regime [15].

1.3.1 Pulsed and Continuous Laser

Depending on the technicality of the processes involved in generating a laser, one can produce a continuous or pulsed laser. The fundamental distinction between a continuous and pulsed laser lies in the rate at which atoms are been populated in the metastable state. When there exists an appreciable time between when population inversion occurs to when Boltzmann law acts (Boltzmann law favours the reversal of population inversion), a pulsed laser will be generated instead of a continuous laser. [18].

Continuous lasers are lasers whose outputs are essentially constant over time, i.e their output power is steady when averaged over any time period. They have time durations in few nanoseconds or less. For a continuous laser operation, it is required for the population inversion of the gain medium to be continually replenished by a steady pumping source, in order to ensure a steady streaming of wave called 'continuous laser'. Not all active medium can be subjected to such steady pumping, because an excessive heat will be generated that will destroy the active medium. Examples of lasers that can be runned in the continuous mode include Argon lasers and CO_2 lasers [18].

Pulsed lasers are those whose output occurs as flashes of light. Of course, one can turn a continuous laser into a pulsed laser by intentionally turning it on and off at some rate in order to create pulses of light. This means that the optical power of a pulsed laser appears in flashes/pulses of some duration at some repetition rate. The energy of a pulsed laser is expressed as the average energy of the laser divided by their repetition rate. By lowering the repetition rate, one can build more energy within a pulse. Pulsed lasers are particularly useful in applications were large amount of energy is required to be delivered in short time. This explains why researchers prefer to use pulsed laser because all the power of a laser appears to be concentrated within a pulse. In this thesis we will make use of pulsed laser. Techniques such as *Q-switching, Mode-locking* and *Pulsed-pumping*

have been used to generate pulsed lasers. Among these techniques, the mode locking technique is most relevant to us. Ti:sapphire is an active medium used in the generation of mode-locked lasers. Ti:Sapphire has a very wide gain bandwidth and can thus produce pulses of only a few femtoseconds duration. Mode-locked laser is a versatile tool for researching processes occurring on extremely short time scales and for maximizing the effect of non-linearity in high harmonic generation [18].

Figure **??** is the diagrammatic representation of a continuous and pulsed laser. The form of the laser in Figure **??**a is $E_o \sin(\omega t + \phi)$ (continuous laser). Observe that all the cycles are of equal amplitude E_o. Figure **??**b represents a 6-cycle pulsed laser ($E_o f(t) \sin(\omega t + \phi)$), with a period T, of 10 fs and a pulse duration, T_p of 50 fs and Full Width of Half Maximum (FWHM) τ, of 4.2 fs. Observe that the amplitude, E_o of each cycle is not uniform but modulated by the envelope, $f(t)$. The amplitude rises starting from the first cycle until its maximum, E_o, then followed by a decrease.

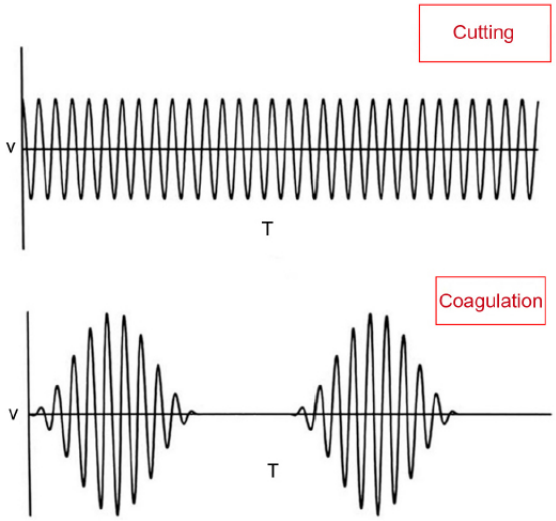

Figure 1.5: A continuous and pulsed laser: (a)represents a continuous laser. (b) represents a 2-pulsed laser containing 10 cycles each[21].

1.3.2 Mathematical Representation of a Laser Field

As already pointed out, a laser is a form of light, and as such it is an electromagnetic waves consisting of a magnetic ($\vec{B}$) and an electric ($\vec{E}$) component. Here $\vec{B}$ and $\vec{E}$ vibrates at mutual right angles to each other as observed in Figure 1.6. The combined field propagates along the z-direction transferring the energy of the system along the same direction, see Figure 1.6. This amount of energy can be quantified by a term called the Poyting vector $\vec{S}(\vec{r}, t)$, given by;

$$\vec{S}(\vec{r}, t) = \frac{1}{u_o} \left(\vec{E} \times \vec{B} \right) \vec{k} \tag{1.5}$$

where u_o is perameability of free space. Mathematically, the components of a laser field can be represented as follows [17].

$$\vec{E}(\vec{r}, t) = E_0 \sin(\omega t - kz + \phi)\vec{i} \tag{1.6}$$

$$\vec{B}(\vec{r}, t) = B_0 \sin(\omega t - kz + \phi)\vec{j} \tag{1.7}$$

$$\vec{B}(\vec{r},t) = -\frac{E_0}{c}\sin(\omega t - kz + \phi)\vec{j} \tag{1.8}$$

Where, $B_0 = -\frac{E_0}{c}$, $\vec{r} = x\vec{i} + y\vec{j} + z\vec{k}$, and $\vec{i}$, $\vec{j}$, $\vec{k}$ are the unit vectors along x, y, z axis, respectively

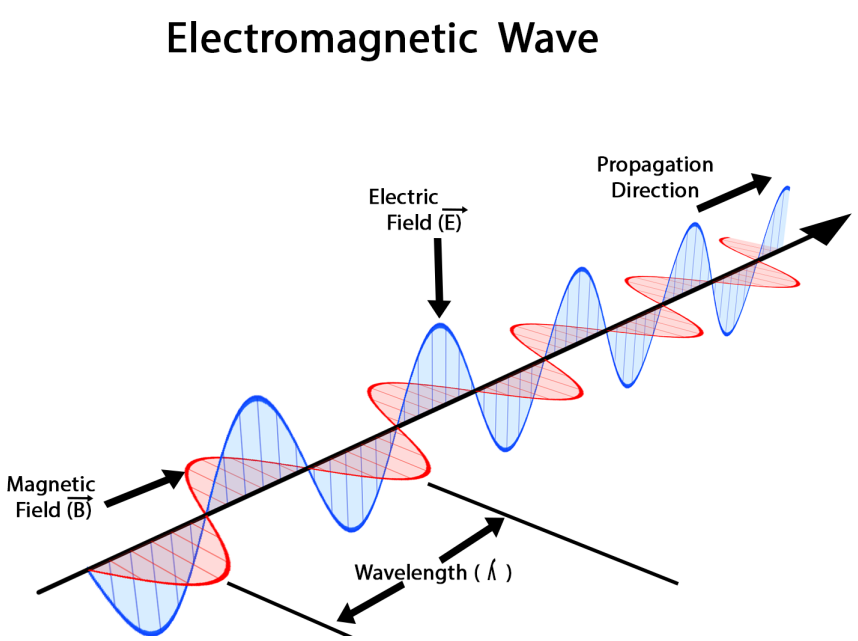

Figure 1.6: Electromagnetic field. Consisting of an electric field $\vec{E}$ vibrating in a perpendicular direction to the magnetic field $\vec{B}$ [9].

The electric component $\vec{E}$ vibrates along the x-axis and propagates along the z direction. While the magnetic component $\vec{B}$ vibrates along the y-axis propagates along the z direction as with $\vec{E}$. Note that the Force due to an electromagnetic field is given by;

$$\vec{F} = q(\vec{E} + v \times \vec{B}) \tag{1.9}$$

where v is the velocity of the particle of charge q, $\vec{E} + v \times \vec{B}$ represents the combined the effect of the combined field. By using Eq.1.6 and Eq.1.8 one obtains;

$$\vec{E} + v \times \vec{B} = E_0 \sin(\omega t - kz + \phi)\left[\vec{i} - \frac{v}{c} \times \vec{j}\right] \tag{1.10}$$

In simplifying Eq.1.10, the following dipole assumptions are made [11].

- Contributions from $\vec{B}$ is neglected
- The positional dependency of the field is neglected

For a laser whose intensity falls in the range of 10^{13} and 10^{14} W/cm^2, the velocity of the electrons driven by the EM field will be far less than the speed of light i.e ($v << c$). Since $\frac{v}{c}$ is associated with $\vec{B}$, then this contribution to the total field will be insignificant. It turns out that Eq.1.10 reduces to

$$\vec{E}(\vec{r},t) = E_0 \sin(\omega t - kz + \phi)\vec{i} \tag{1.11}$$

For lasers whose wavelength is of the order of $10^{-9}m$, $\vec{E}$ will appear constant over the extension of one atom. Thus the z-component dependency can be ignored. This justification follows from the fact that the wavelength of visible - near infra-red light is much bigger than the size of an atom (10^{-15} m). Finally, Eq.1.11 becomes;

$$\vec{E}(t) = E_0 \sin(\omega t + \phi)\vec{i} \tag{1.12}$$

Eq.1.12 represents the form of the incident laser field needed to generate High Order Harmonics. The field is linearly polarized along the x-direction, E_0 represents its amplitude. In a continuous laser, E_0 is constant over the entire length of the laser field. However in a pulsed laser, E_0 is modulated by an additional term $f(t)$ refereed to as the envelope of the field. In general a pulsed laser is defined by:

$$\vec{E}(t) = E_0 f(t) \sin(\omega t + \phi)\vec{i} \tag{1.13}$$

where the Carrier Envelope Phase, ϕ was set to zero in our simulation, and the frequency ω is given by:

$$\omega = \frac{2\pi c}{\lambda} \tag{1.14}$$

Specifically, the envelope $f(t)$ of the laser field can take the following form [22]:

$$f(t) = \begin{cases} \sin^2(\frac{\pi t}{T_p}), & \text{Sine form} \\ e^{-2ln2\frac{\tau^2}{t^2}}, & \text{Gaussian from} \end{cases} \tag{1.15}$$

$$T_p = n_c \times T \tag{1.16}$$

Where, T is the period of a cycle, T_p is Pulse length of the laser field, τ is Full Width of Half Maximum (FWHM). For our simulation, the following laser form have been used.

$$E(t) = E_o \sin^2\left(\frac{\pi t}{n_c \times T}\right) \sin\left(\frac{2\pi c}{\lambda} t\right) \tag{1.17}$$

1.3.3 Properties of a Laser

Lasers have fascinating properties that no other light sources possess. They represent a well uniform collection of identical photons. There are four (4) commonly known properties of lasers, which are *coherency* of their photons, *monochromaticity* of its frequency, *directionality* of their beam and its *high intensity*. These properties are briefly summarized below [18];

- Coherency: Lasers like any other light are made up of photons. Unlike in other light sources, the constituent photons in lasers are properly aligned with each other. They possess a fixed phase relationship one to another. i.e ϕ is the same for all the photons.

- Monochromaticity: The photons of a laser do not only have identical phase relationship, but also have a single frequency, ω. No two colours exist in a typical laser.

- Directionality: They appear as narrow beams with an extremely small beam diameter. This directional property is supported by the close stacking of the photons. So, laser beam can travel long distances in a seemingly straight path. Thus exhibiting spatial coherency, as well as temporal coherency.

- High intensity: Laser intensity is the amount of energy transferred by the laser through a region of space per unit time. Its derivation can be obtained by taking the time average of the moduli of the Poyting vector [11]. i.e.

$$I = \langle S \rangle = \frac{1}{T} \int_0^T |\vec{S}| \; dt \tag{1.18}$$

From Eq.1.5 one gets:

$$|\vec{S}| = \frac{1}{u_o} \left| \vec{E} \times \vec{B} \right| \tag{1.19}$$

$$= \frac{1}{u_o} |\vec{E}|.|\vec{B}| \sin(\frac{\pi}{2}) \tag{1.20}$$

By considering a pulsed laser, and putting Eq.1.5 and Eq.1.8 into Eq.1.20 and note that the fields are position independent, we get

$$= \frac{E_o^2}{u_0 c} f^2(t) \sin^2(\omega t + \phi) \tag{1.21}$$

Taking into account the fact that $c^2 = \frac{1}{u_0 \epsilon_o}$, Eq.1.21 becomes;

$$|\vec{S}| = c\epsilon_o E_o^2 f^2(t) \sin^2(\omega t + \phi) \tag{1.22}$$

Substituting Eq.1.22 into Eq.1.18 we have

$$\langle S \rangle = \frac{c\epsilon_o E_o^2}{T} \left\langle f^2(t) \right\rangle \int_0^T \sin^2(\omega t + \phi) \, dt \tag{1.23}$$

We shall shortly see in the next chapter that the average of $f^2(t)$ defined as $\langle f^2(t) \rangle$, is given by $\langle f^2(t) \rangle = 1$

$$\therefore \; \langle S \rangle = \frac{c\epsilon_o E_o^2}{T} \int_0^T \frac{1}{2} \left[1 - \cos(\omega t + \phi) \right] dt$$

$$= \frac{c\epsilon_o E_o^2}{T} . \frac{T}{2}$$

Therefore, the laser intensity, I is given as;

$$I = \frac{c\epsilon_o E_o^2}{2}$$

The amplitude of the laser field, E_o in Eq.1.17 can now be expressed as

$$E_o = \sqrt{\frac{2I}{c\epsilon_o}} \tag{1.24}$$

CHAPTER 2

HIGH-ORDER HARMONIC GENERATION

2.1 Models of HHG process

The advent of ultrashort fields like lasers (femtoseconds laser) has opened the door to a lot of interesting phenomena which hitherto could not have been accessed using ordinary light [3]. But as advances continues in science, the need to probe deeper into intra-atomic and intra-molecular region arose. Quite a number of methods have been employed to produce shorter pulses needed for this action. But HHG process has been embraced by the attosecond research community, as an economical way to produce shorter pulses (in the attoseconds ($10^{-18}s$) and zeptoseconds($10^{-27}s$) time scale) [1]. The HHG process is a non-linear process that produces higher energy multiple of the energy of an incident photon. When photon of energy E_{iph} interacts with an atom, it will emit a photon of energy E_{eph} in an harmonic order of the incident photon [2], as per:

$$E_{\text{eph}} = N.E_{\text{iph}} \tag{2.1}$$

where N, represents the harmonics of the of the incident laser. They occur as odd integers [21]. Typically, harmonic orders of 30 - 70 have been obtained using a 800 nm, laser of intensity $2 - 5 \times 10^{14} W/cm^2$ [**?**]. The Figure 2.1 shows the experimental set up used for an HHG process.

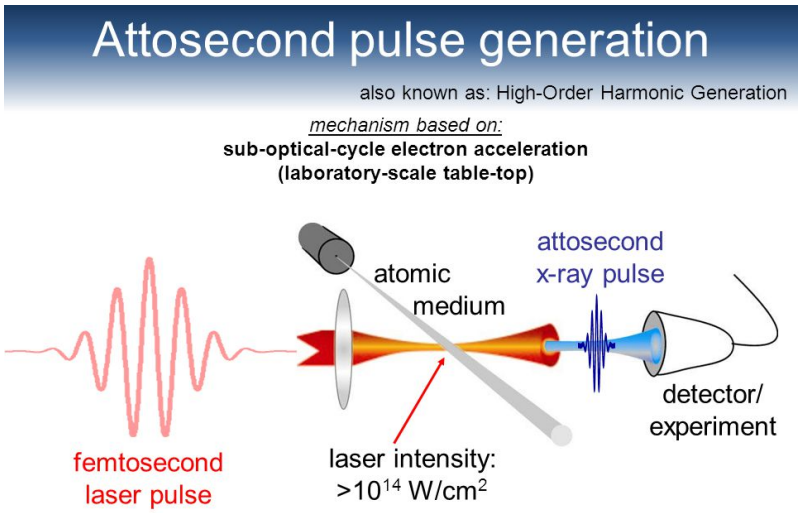

Figure 2.1: Experimental set up for HHG production[18].

Given a 5-cycle pulsed laser as shown in Figure 2.2, attoseconds pulses will be generated from each half cycle, thereby amounting to a train of attosecond pulses [16].

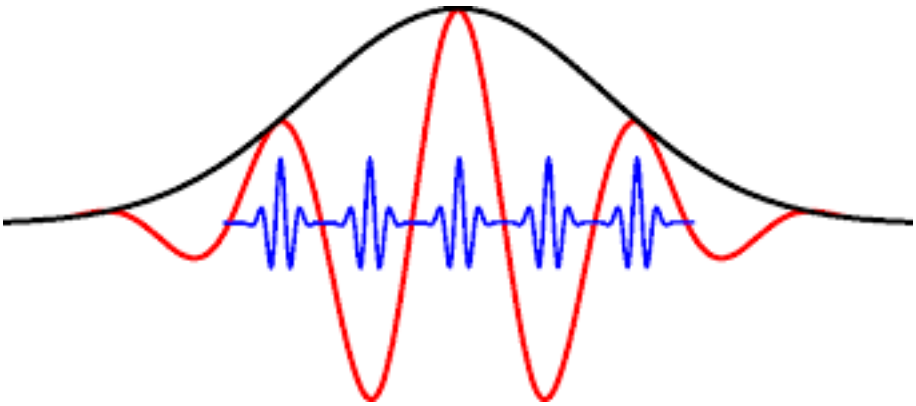

Figure 2.2: Train of attoseccond pulses[1].

It is important to emphasize the observation of noticeable changes in the intensity, $I(W/cm^2)$, energy $E(eV)$, and time scale $t(s)$, of the generated harmonics. The energy of the radiated photon shifts from the near infra red region into the ultraviolet region of the spectrum. The femtosecond time scale of the incident/driving field is converted into the attoseconds time scale of the high-order harmonics coupled with intensity enhancement. [16].

By considering the single atom response of HHG process (also called *microscopic high harmonic generation*) [17], all the above notable changes of the high harmonics are still achievable. But in a real system consisting of several atoms, all the possible harmonics from each atom will add up together through phase matching to increase the intensity of the harmonic . This holistic consideration is called the *macroscopic high harmonic generation* [14]. Our consideration for the rest of this work shall be on the microscopic high generation process. Models have been established which seek to explain in details the microscopic generation process. The 3-step model (refereed to as *The simple Man-Model*), and the Lewestein model (also called *The Strong Field Approximation (SFA) Model*), as well as the Direct integration of the TDSE[1] are currently known models. The 3-step model combines a classical and quantum physics approach to explain the HHG process, while the SFA Model is a pure Quantum mechanical description. The Direct integration of the TDSE proves to be a fast technique able to produce the HHG spectrum.

2.1.1 The simple Man-Model

The simple Man-Model was the earliest model developed by Krause, Schafer and Corkum used to explain high harmonics generation from a linearly polarised and moderately intense laser field (10^{13} - 10^{14} W/cm^2) [21].

Consider an electron confined to a soft-core potential (as shown in Figure 2.3). Under the influence of a laser field, the arms of the potential will be suppressed allowing the electron to escape. The free electron will travel through the free space around the soft core. Due to the influence of the oscillating nature of the driving field, the electron will be brought back to recollide with the soft-core. And as before, the shape of the soft-core potential changes facilitating ionization and subsequent recollision. This action continues on and on, generating attoseconds pulse at each recollision [2]. This process has been conviniently divided into three (3) stages: ionization, propagation and recombination.

[1]TDSE: Time Dependent Schrödinger Equation

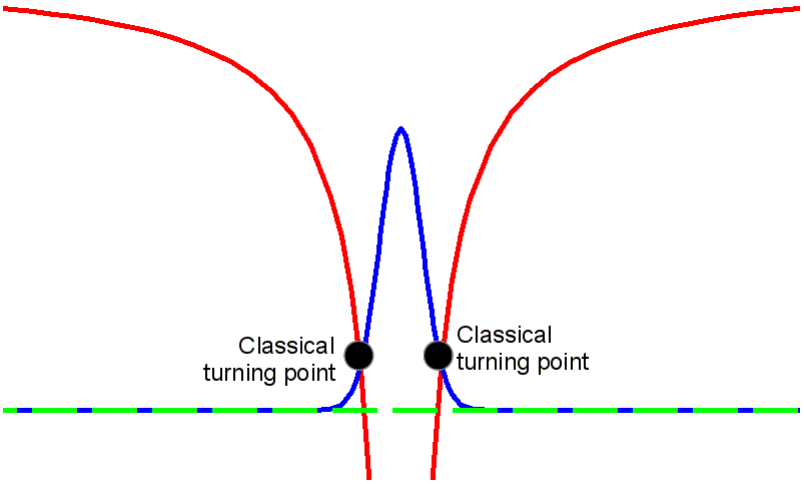

Figure 2.3: An electron wavepacket (blue) confined in a soft core potential (red), the dots indicate the two classical turning points[16].

- Ionization : Ionization is the first step in the 3-step model. An electron that is initially confined to coulombic barrier whose height is characterized by ionization potential, I_P, will escape, due to the energy supplied to the electron from the laser field. This escape can occur in one of the three (3) ways namely: multiphoton ionization, barrier suppresed ionization and tunneling ionization. Each of these process can be classified based on the value of their keldysh parameter, γ, defined as:

$$\gamma = \sqrt{\frac{I_P}{2U_P}} \tag{2.2}$$

  where, U_P is the Ponderomotive Energy (maximum kinetic energy gained by the electron as it travels freely in the continumm). It follows from Eq.2.2 and Eq.1.24 that U_P scales directly as the intensity of the driving field.

  - Multiphoton ionization ($\gamma >> 1$): Occurs when the ponderomotive energy U_P is much smaller than the ionization potential I_P of the atom, thus the Coulomb potential will be weakly distorted. So, inorder for the electron to escape the coulombic attraction, it will absorb a certain number of the incident photon.
  - Barrier suppressed ionization ($\gamma << 1$): Occurs when U_P greatly exceeds I_P, thereby completely suppressing the Coulomb barrier that originally confined the electron. The entire electron leaks away from the ion and enters directly into continuum states, due to the strong laser field.
  - Tunnelling ionization ($\gamma \approx 1$): Occurs when the strenght of U_p approaches I_p. In such a case, the coulomb potential is significantly distorted, thereby creating a finite barrier through which a portion of the electron wavepacket can tunnel. Ionization of this kind is a quatum mechanical phenomena, which happens to be a relevant regime for producing High-order Harmonics [1].

  Consider a single-cycle laser shown in Figure 2.4. If the phase of the driving laser interacting with the soft-core falls within $[0, \frac{\pi}{2}]$ the recombination will occur within $[\pi, \frac{3\pi}{2}]$ [17].

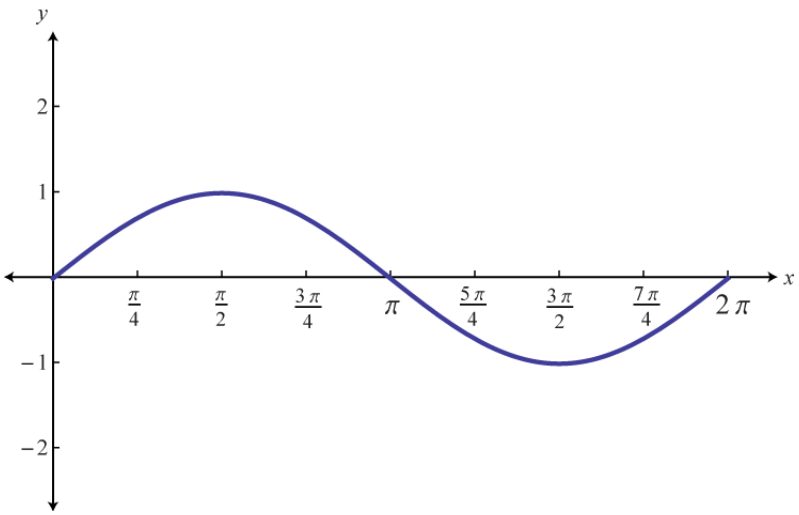

Figure 2.4: A single cycle sine wave laser

- Propagation: Once the electron is ionized, it quickly escapes the short-range potential of the ion whereupon the laser potential dominates. The electron taken away from the atom is accelerated by the laser field in the direction perpendicular to the optical axis of propagation of the laser beam [1]. The motion of the electron following ionization can then be classically modeled. The Hamiltonian of the electron propagating along the x-direction is given by:

$$H(t) = T + V \tag{2.3}$$

where T is kinectic energy, V the potential experienced by the electron are given by:

$$T = \frac{P^2}{2m} \tag{2.4}$$

$$V = -\int E(t)dx \tag{2.5}$$

and from the electric field $E(t)$ given by:

$$E(t) = f(t)E_o \sin(\omega t + \phi) \tag{2.6}$$

one gets:

$$\therefore V = -ef(t)E_o \sin(\omega t + \phi) \int dx$$

$$V = -exf(t)E_o \sin(\omega t + \phi) \tag{2.7}$$

Putting Eq.2.4 and Eq.2.7 into Eq.2.3, we get:

$$H(x,t) = \frac{P^2}{2m} - exE_o f(t) \sin(\omega t + \phi) \tag{2.8}$$

Using the Hamilton equation in 1D we obtain:

$$m\frac{d^2x}{dt^2} = \frac{dP}{dt} = -\frac{\partial H(x,t)}{\partial x} \tag{2.9}$$

Inserting Eq.2.8 into Eq.2.9, one gets:

$$m\frac{d^2x}{dt^2} = -\frac{\partial}{\partial x}\left[\frac{P^2}{2m} - exE_o f(t)\sin(\omega t + \phi)\right]$$

Thus, by considering $m = 1$, the acceleration of the ionized electron $a(t)$ is described by:

$$a(t) = \frac{d^2x}{dt^2} = E_o f(t)\sin(\omega t + \phi) \tag{2.10}$$

The velocity $v(t)$ is given by:

$$v(t) = \int_{t_i}^{t} a(t)dt \tag{2.11}$$

$$v(t) = \int_{t_i}^{t} E_o f(t)\sin(\omega t + \phi)dt \tag{2.12}$$

Where t_i is ionization time, t_p is propagation time assume $t_i = 0$, Eq.2.12 reads:

$$v(t) = -\frac{E_o}{\omega} f(t)\cos(\omega t + \phi) + v_d \tag{2.13}$$

Where v_d is the constant of integration (representing the drift velocity of the electron during ionization)

$$x(t) = \int_{t_i}^{t} v dt = \int_{0}^{t} v dt \tag{2.14}$$

So, the trajectory of the electron is

$$x(t) = -\frac{E_o}{\omega}\int_0^t \left[f(t)\cos(\omega t + \phi) + v_d\right] dt$$

$$x(t) = -\frac{E_o}{\omega} f(t)\sin(\omega t + \phi) + v_d t + x_o \tag{2.15}$$

Where t is the recombination time and x_o, the initial position (integration constant), assume the electron starts at the origin. A plot of its trajectory is shown in Figure 2.5. For a variety of ionization phases, only ionization phases within $[0, \frac{\pi}{2}]$ give trajectories that return to the origin, leading to recollision.

- Recombination: The recombination step provides the mechanism for the electron to release its kinetic energy through photon emission. We have already seen that not all electron trajectories end at the core. In such instances, the electron become absolutely free, and travel with very high energy. [4]. For trajectories relevant to HHG, the electron returns to the core. Upon recombining with the core, the total

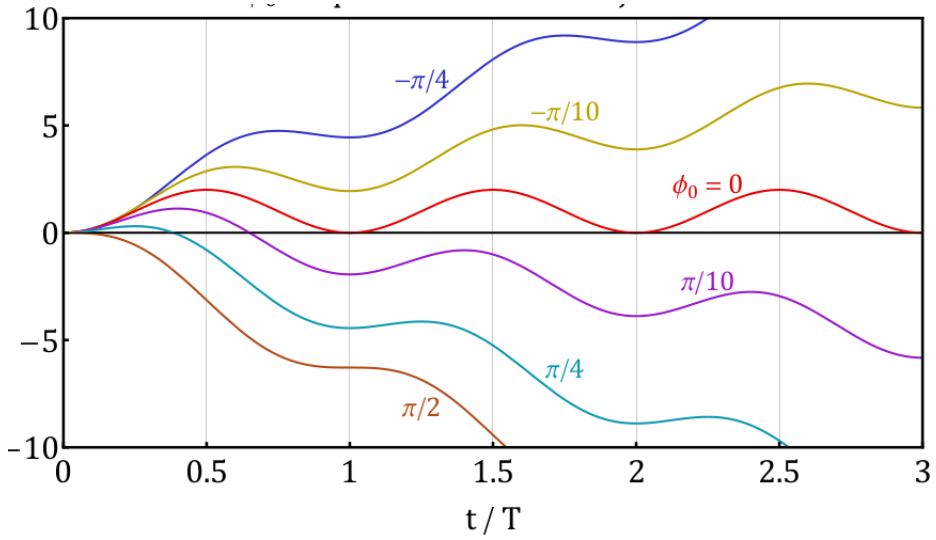

Figure 2.5: Electron trajectory in a linearly polarised laser field.

kinetic energy acquired by the propagating electron[2] E_k is released together with the electron's potential energy, I_p [14], to produce attosecond pulses,whose energy is E is given as:

$$E = NE_{iph} = I_p + E_k \tag{2.16}$$

where;

$$E_k = \langle E_k \rangle = \frac{1}{2} m \left\langle v^2(t) \right\rangle \tag{2.17}$$

and,

$$\left\langle v^2(t) \right\rangle = \frac{1}{T} \int_0^T v^2(t) dt \tag{2.18}$$

$$\left\langle v^2(t) \right\rangle = \frac{1}{T} \int_0^T \left[\frac{E_o^2}{\omega^2} f^2(t_p) \cos^2(\omega t_p + \phi) - \frac{E_o v_d f(t_p)}{\omega} \cos(\omega t_p + \phi) + v_d^2 \right] dt$$

$$\left\langle v^2(t) \right\rangle = \frac{1}{T} \left[\frac{E_o^2 f^2(t_p)}{2\omega^2} T + v_d^2 T \right]$$

$$\left\langle v^2(t) \right\rangle = \frac{E_o^2 f^2(t_p)}{2\omega^2} + v_d^2$$

$\therefore$ (2.17) becomes

$$\langle E_k \rangle = \frac{E_o^2 f^2(t_p)}{4\omega^2} + \frac{v_d^2}{2} \tag{2.19}$$

For $\langle E_k \rangle$ to be maximum, then, $v(t) = 0, \quad f(t_p) = 1 = \cos(\omega t_p + \phi)$,

[2]In the simulation, the electron's kinetic energy is treated as a sum of its intrinsic potential energy and the kinetic energy gained during propagation. See Chapter 4 for details

$$\therefore v_d = -\frac{E_0}{\omega} \tag{2.20}$$

(2.19) now become

$$\langle E_k \rangle = \frac{E_0^2}{4\omega^2} + \frac{E_0^2}{2\omega^2} \tag{2.21}$$

$$\langle E_k \rangle = \frac{3E_0^2}{4\omega^2} \tag{2.22}$$

If we define U_p, as $U_p = \frac{E_0^2}{4\omega^2}$, then

$$\langle E_k \rangle = 3U_p \tag{2.23}$$

(2.16) becomes

$$E = I_p + 3U_p \tag{2.24}$$

This result approximately[3] corresponds to experimental findings, given by;

$$E = I_p + 3.17U_p \tag{2.25}$$

$$N\hbar w_c = I_p + 3.17U_p \tag{2.26}$$

w_c is the maximum frequency of the emitted photon (cut- off frequency).
We observe that the energy of the maximum frequency w_c in a HHG spectrum depends on the kinetic energy of the recombining electron and to the binding-energy gained while tunnelling.

One can clearly see in Figure 2.6 a pictorial summary of the HHG process occurring within a cycle of a pulsed laser. An electron initially at rest can be ionized between $(0 - 0.25T)$ the time interval of the laser field (corresponding to 0 - $\frac{\pi}{2}$). During ionization, the right arm of the soft-core deflects downward, while the left arm is elevated thereby allowing the electron to escape from its confinement in a process called tunnelling ionization, with the strongest ionization occurring at $0.25T$ (corresponding to $\frac{\pi}{2}$). Upon tunnelling, the electron leaves the core and travels in the continuum. When the field changes its sign, the arm suppression reverses, thereby accelerating the electron back to the core (in our simulation, the arms of the soft-core was long enough to contain the motion of the electron). The recombination occurs between the time interval $0.5T - 0.75T$ of the dipole acceleration (corresponding to π - $\frac{3\pi}{2}$).

As a step to calculate the HHG spectrum, lets take the fourier transform [1] of (2.10);

$$a(\omega) = \frac{1}{2\pi} \int_0^{T_p} dt \;\; a(t) e^{-i\omega t} \tag{2.27}$$

The HHG spectrum, $S(\omega)$ is given [25] as:

$$S(w) = |a(w)|^2 \tag{2.28}$$

$$S(w) = \left| \frac{1}{2\pi} \int_0^{T_p} dt \;\; a(t) e^{-i\omega t} \right|^2 \tag{2.29}$$

[3]This is because we have considered, that all electron motion resulting to HHG are ionized at $t_i = 0$, but in real situation $0 < t_i < 0.25T$

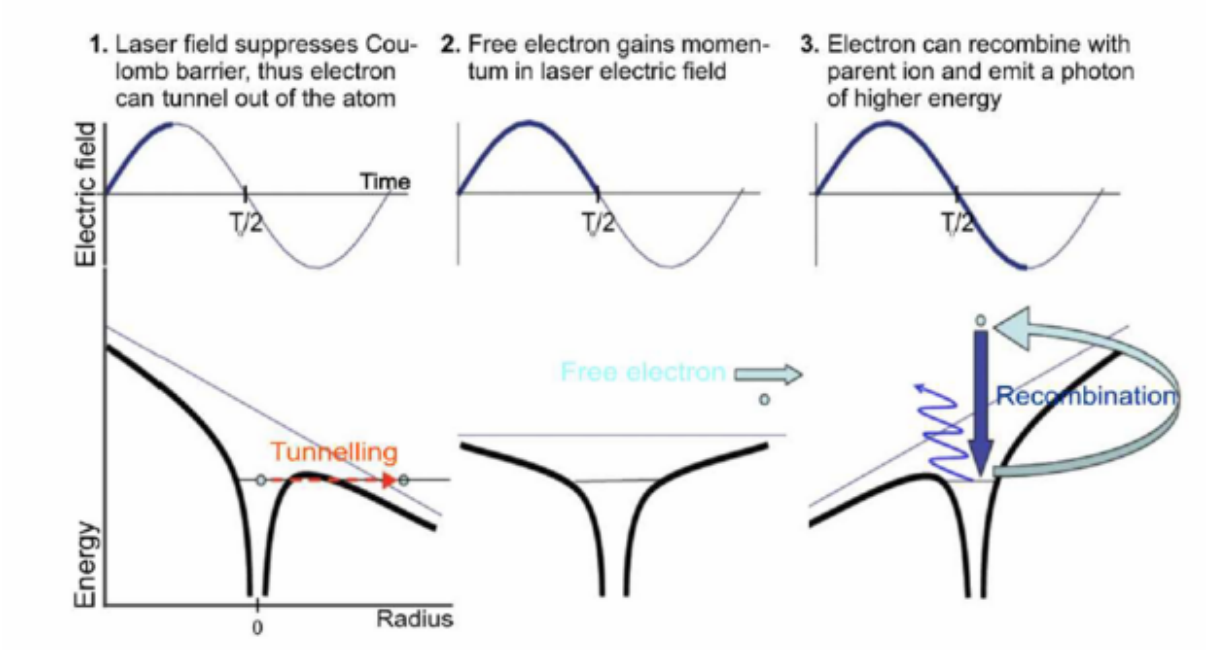

Figure 2.6: The 3-step HHG process. The laser field controls the suppression of the soft-core potential arms. This suppression in turn controls the motion of the electron[14].

This model breaks down in the presence of elliptical fields. With a circularly polarized field (an example of elliptical fields), the returning electron would miss its target (core), because quantum mechanically, the overlap of the returning electron wavepacket and the nuclear wavepacket is reduced [1]; as such, harmonic photon will not be generated. But now it has been shown that elliptically polarized fields are capable of supporting HHG process by mixing two colors of circularly polarized light[5]. As an extension of the Simple Man-Model, Milosevic successfully generated HHG spectrum with a field vibrating in two (2) axis direction. The equation below gives the form of polarized light used by Milosevic

$$E(t) = \frac{1}{2i}\left[\frac{E_1}{\sqrt{1+\epsilon_1^2}}(\hat{x} - i\epsilon_1\hat{y})e^{i\omega_1 t} + \frac{E_2}{\sqrt{1+\epsilon_2^2}}(\hat{x} - i\epsilon_2\hat{y})e^{i\omega_2 t}\right] + c.c \tag{2.30}$$

where $\hat{x}$, $\hat{y}$ are unit vectors of the polarization direction x,y respectively axis of polarization. Here $\omega_2 = 2\omega_1$, $\epsilon_1 = \epsilon_2 = 1$ (two corotating circularly polarized field), $\epsilon_1 = \epsilon_2 = -1$ (two counter-rotating circularly polarized field).

Fields of higher intensity ($> 10^{16}\ W/cm^2$) do not give rise to HHG. At such intensities, the speed of the electron, v will approach the relativistic value c, i.e. $v = c$

This implies that the magnetic component that was initially ignored in our earliest derivation of the laser field form in Chapter 1, will now contribute significantly to the laser field. The presence of the magnetic field ($\vec{B}$), will give rise to Lorentz force $\vec{F_L}$

$$\vec{F_L} = m\frac{d\vec{v}}{dt} = e\left(\vec{E} + \vec{V} \times \vec{E}\right) \tag{2.31}$$

capable of causing an excessive suppression of the soft core potential. In this case, the electrons get ionized through the *Barrier Suppressed Regime*. Figure 2.6 describes the the response of the soft-core potential to fields higher than $10^{16}\ W/cm^2$

The whole electron wavepacket leaves the soft-core and enters into the continuum. As earlier mentioned, HHG will occur when the returning electron wavepacket interacts with the remainder of the electron wavepacket in the bound state of the soft-core. Since in the case of the intensity higher than $10^{16}\ W/cm^2$ intensity, the whole electron wavepacket leaks out from the core, then HHG can not be realized in this intensity regime [17]. However models have been employed that explains the possibility of achieving HHG even in the presence of Lorentz force $\vec{F_L}$. The scope of this research will apply only to moderate intense and linearly polarized field.

2.1.2 The Strong Field Approximation (SFA) Model

The Strong Field Approximation (SFA) is a full quantum mechanical description of the HHG process. The basic equation of this theory is the time dependent Schrodinger's equation (TDSE) [16].

$$\left[-\frac{\hbar^2}{2m}\frac{\partial^2}{\partial r^2} + V(\vec{r},t)\right]|\Psi(\vec{r},t)\rangle = i\hbar\frac{\partial}{\partial t}|\Psi(\vec{r},t)\rangle \tag{2.32}$$

where $V(\vec{r},t) = V_{\text{at}}(r) + V_{\text{laser}}(r,t)$, is made of the coulomb potential $V(r) = -\frac{1}{r}$, and the laser potential $V_{\text{laser}} = -exE_o\cos(\omega t + \phi)$, Eq.2.32) becomes:

$$\left[-\frac{\hbar}{2m}\frac{\partial}{\partial r} + V_{\text{at}}(r) - exE_o\cos(\omega t + \phi)\right]|\Psi(\vec{r},t)\rangle = i\hbar\frac{\partial}{\partial t}|\Psi(\vec{r},t)\rangle \tag{2.33}$$

Given the following SFA assumption;

- Only the $|0\rangle$ bound state (ground state) contributes to the the evolution of the atomic system, while all other states contributions are neglected.
- The depletion of the ground state, $|0\rangle$, is ignored.
- Once the electron ionizes to a continuum state, $|p\rangle$ the short-range atomic potential $V_{\text{atomic potential}}(r)$ no longer acts on it.

The solution to Eq.2.33 is :

$$|\Psi(\vec{r},t)\rangle = e^{iI_p/\hbar}\left[a(t)|0\rangle + \int d^3\vec{p}\ b(\vec{p},t)\right]|p\rangle \tag{2.34}$$

where $a(t)$ is the portion of the wavefunction that stays in the ground state and is given by

$$a(t) = 1 \tag{2.35}$$

$b(t)$ the portion of the wavefunction that ionizes and enters the continuum state

$$b(\vec{p},t) = \frac{i}{\hbar}\int_0^t dt' eE_o\cos(\omega t')d_y(\vec{p} - eA(t'))e^{-iS(\vec{p},t,t')} \tag{2.36}$$

where $S(\vec{p},t,t')$ is the Semi-classical action (defining the trajectory of the electron)

$$S(\vec{p},t,t') = \frac{1}{\hbar}\int_{t'}^t dt''\left[\frac{(\vec{p} - eA(t''))^2}{2m} + I_p\right] \tag{2.37}$$

The dipole moment d_m of the electron reads:

$$d_m(t) = \langle \Psi(\vec{r},t)| \, y \, |\Psi(\vec{r},t)\rangle \tag{2.38}$$

Puting Eq.2.35, Eq.2.36, Eq.2.37 into Eq.2.38 results to:

$$d_m(t) = \int d^3\vec{p} \; b^*(\vec{p},t) \, \langle \vec{p}| \, y \, |0\rangle + \;\; c.c \tag{2.39}$$

Finally, we get:

$$d_m(t) = \frac{i}{\hbar}\int_o^t dt' \int d^3\vec{p} e E_o \cos(\omega t') d_y(\vec{p} - eA(t')) e^{-iS(\vec{p},t,t')} d_y^*(\vec{p} - eA(t)) + c.c \tag{2.40}$$

Ionization, propagation and recombination can be explained using (2.40) as follows [3]:

- Ionization: An electron is ionized at time t' from the bound state into the continuum state with a probability amplitude; $eE_o \cos(\omega t') d_y(\vec{p} - eA(t'))$
- Propagation: During its flight (from t' to t), the electron is considered as a particle moving freely in the laser electric field and therefore the wavefunction describing the electron acquires an additional phase factor $e^{-iS(\vec{p},t,t')}$.
- Recombination: Finally, the electron recombines with the ion at time t, transitioning from a continuum state to the bound state with a probability amplitude: $d_y^*(\vec{p} - eA(t))$

The resulting dipole acceleration $d_a(t)$ is given by:

$$d_a(t) = \dot{d_m}(t) \tag{2.41}$$

The emission amplitude into the N^{th} harmonic with frequency$N\omega$ reads:

$$E = \int_{-\infty}^{\infty} dt e . d_a(t) e^{-iN\omega t} \tag{2.42}$$

It is important to note that E which represents the energy of the emitted photon as calculated by ths model is given by:

$$E = \alpha I_p + 3.17 U_p \tag{2.43}$$

Where $\alpha = 1.32$. It is larger than the value obtained with the Simple-man model because the quantum calculations involve wave-packet spreading (spatial extension of the wave function) [23].

2.1.3 Direct integration of the TDSE

This is one of the most straightforward approach to investigate HHG process involving the numerical solution of the TDSE. This approach provides us with exact numerical solutions, and in this thesis, the TDSE will be solved using the Fast Fourier Transform (FFT) Split Operator Method. It is important to note that, the effect of the atomic coulomb potential which was neglected during the propagation stage in section (2.1.2) is taken into account in this model [21].

We shall adopt the direct integration of the TDSE in our research to generate the HHG spectrum, while the semi-classical model shall be employed to verify the results that follows.

2.1.3.1 The Split Operator Method

The split operator method is a spectral method developed by Feit and Fleck to solve the TDSE [24]. This is an extremely fast technique that relies on computing the solution in small steps with a high accuracy, thereby making this method particularly attractive for application with the spectral method to the Schrödinger equation in Cartesian coordinates. $\Psi(x,t)$ which carries information regarding the *dynamics of the electron* is obtained from the Split operator method. In this subsection, we shall provide detailed derivation of $\Psi(x,t)$ by analytically solving the TDSE. For a 1-D consideration, the TDSE is given by;

$$i\hbar\frac{d}{dt}\left|\Psi(x,t)\right\rangle = \hat{H}\left|\Psi(x,t)\right\rangle \tag{2.44}$$

where,

$$\left|\Psi(x,t)\right\rangle = U(t,t_o)\left|\Psi(x,t_0)\right\rangle \tag{2.45}$$

$\hat{H}$ is Hamiltonian, $U(t,t_o)$ is Evolution Operator, t_o is initial time, t is some later time, $|\Psi(x,t_o)\rangle$ is initial wavefunction. The time interval Δt reads:

$$\Delta t = t - t_o \tag{2.46}$$

and, $|\Psi(x,t)\rangle$ is given by:

$$\left|\Psi(x,t)\right\rangle = U(t,t_o)\left|\Psi(x,t_o)\right\rangle \tag{2.47}$$

We now proceed to solve Eq.(2.44) using the Split Operator Method. This method involves spiting the $\hat{H}$ of the system as a sum of two operators (namely the kinetic energy operator and potential energy operator) [24]. Inserting Eq.2.47 into Eq.2.44 yields:

$$\left|\Psi(x,t_o)\right\rangle i\hbar\frac{d}{dt}U = \hat{H}U(t,t_o)\left|\Psi(x,t_o)\right\rangle$$

$$i\hbar\frac{dU}{dt} = \hat{H}U(t,t_o)$$

$$\int\frac{dU}{U} = -i\frac{\hat{H}}{\hbar}\int_{t_o}^{t}dt$$

$$\ln U = -i\frac{\hat{H}}{\hbar}t$$

$$U(t,t_o) = e^{-\frac{i}{\hbar}\hat{H}(t-t_0)} \tag{2.48}$$

$\therefore$ Eq.(2.47) becomes;

$$\left|\Psi(x,t)\right\rangle = e^{-\frac{i}{\hbar}\hat{H}\Delta t}\left|\Psi(x,t_o)\right\rangle \tag{2.49}$$

Upon using Eq.(2.46), and noting that $\hat{H} = \hat{T} + \hat{V}$, we get

$$\left|\Psi(x,t_0+\Delta t)\right\rangle = e^{-\frac{i}{\hbar}(\hat{T}+\hat{V})\Delta t}\left|\Psi(x,t_o)\right\rangle \tag{2.50}$$

where $\hat{T}$ is the kinetic energy operator, $\hat{V}$ is the potential energy operator

Next we will use the Baker- Campell-Hausdorfff approximation which is given by:

$$e^{(\hat{T}+\hat{V})\Delta t} = e^{\hat{T}\Delta t}e^{\hat{V}\Delta t}e^{-\frac{\Delta t^2}{2}[\hat{T},\hat{V}]}e^{\frac{\Delta t^3}{6}(2[\hat{V},[\hat{T},\hat{V}]]+[\hat{V},[\hat{T},\hat{V}]])} \tag{2.51}$$

For a small Δt, the third higher order terms becomes negligible, so, Eq.2.51 becomes:

$$e^{(\hat{T}+\hat{V})\Delta t} = e^{\hat{T}\Delta t}e^{\hat{V}\Delta t} \tag{2.52}$$

$\therefore$ Eq.(2.50) now reads

$$|\Psi(x, t_0 + \Delta t)\rangle = e^{-\frac{i}{\hbar}\hat{T}\Delta t}e^{-\frac{i}{\hbar}\hat{V}\Delta t}|\Psi(x, t_o)\rangle \tag{2.53}$$

$$|\Psi(x, t_0 + \Delta t)\rangle = e^{-\frac{i}{2\hbar}\hat{V}\Delta t}e^{-\frac{i}{\hbar}\hat{T}\Delta t}.e^{-\frac{i}{2\hbar}\hat{V}\Delta t}|\Psi(x, t_o)\rangle \tag{2.54}$$

We should quickly note that the $\hat{T}$ operator acts only in the momentum configuration (p), while the $\hat{V}$ operator acts only in the position configuration (x).

Eq.2.54 was numerically solved by employing Fourier Transform. In which case, the wavepacket is transformed between position configuration $\Psi(x, t)$, and momentum configuration, $\Psi(p, t)$, to allow the operators act accordingly [24].

The computational implementation of Eq.2.54 is summarized in the 3 -steps below;

- **Action of $\hat{V}$**: By acting the 3rd exponential term in Eq.2.54, we have

$$e^{-\frac{i}{2\hbar}\hat{V}\Delta t}|\Psi(x, t_o)\rangle = |\Psi(x', t_o)\rangle \tag{2.55}$$

  Eq.2.54 now reduces to

$$|\Psi(x, t_0 + \Delta t)\rangle = e^{-\frac{i}{2\hbar}\hat{V}\Delta t}e^{-\frac{i}{\hbar}\hat{T}\Delta t}.|\Psi(x', t_o)\rangle \tag{2.56}$$

- **Action of $\hat{T}$**: we fourier transform $|\Psi(x', t_o)\rangle$ into momentum space $|\Psi(p, t_o)\rangle$, then by acting the second exponential term in Eq.2.56, it follows that:

$$|\Psi(p, t_o)\rangle = \mathcal{F}(|\Psi(x', t_o)\rangle) = \frac{1}{\sqrt{2\pi}}\int dx\,|\Psi(x', t_o)\rangle\, e^{-i\frac{p}{\hbar}x} \tag{2.57}$$

  Then, Eq.2.56 becomes,

$$|\Psi(x, t_0 + \Delta t)\rangle = e^{-\frac{i}{2\hbar}\hat{V}\Delta t}.e^{-\frac{i}{\hbar}\hat{T}\Delta t}.|\Psi(p, t_o)\rangle = e^{-\frac{i}{2\hbar}\hat{V}\Delta t}.|\Psi(p', t_o)\rangle \tag{2.58}$$

  where $|\Psi(p', t_o)\rangle = e^{-\frac{i}{\hbar}\hat{T}\Delta t}.|\Psi(p, t_o)\rangle$

- **Action of $\hat{V}$:** The last term in the preceeding result Eq.2.58 is in the momentum configuration, in order for $\hat{V}$ to act, we first perform an inverse Fourier on transform $|\Psi(p', t_o)\rangle$ so as to obtain its equivalent in position configuration $(|\Psi(x'', t_o)\rangle)$;

$$|\Psi(x'', t_o)\rangle = \mathcal{F}(|\Psi(p', t_o)\rangle) = \frac{1}{\sqrt{2\pi}}\int dx\,|\Psi(p', t_o)\rangle\, e^{i\frac{p}{\hbar}x} \tag{2.59}$$

So, that Eq.2.58 becomes;

$$|\Psi(x, t_0 + \Delta t)\rangle = e^{-\frac{i}{2\hbar}V\Delta t} |\Psi(x'', t_o)\rangle \tag{2.60}$$

Eq.2.60 represents the final form of electron wave motion.

Set

$$|\Psi(x, t_0 + \Delta t)\rangle = |\Psi(x, t)\rangle \tag{2.61}$$

The obtained wavefunction in Eq.2.60 can be used to compute the average kinectic energy, $\langle E_{kin}\rangle$ and the potential energy, $\langle E_{pot}\rangle$ of the electron. Thus,

$$\langle E_{kin}\rangle = \left\langle \Psi(x,t) \middle| \frac{p^2}{2m} \middle| \Psi(x,t) \right\rangle \tag{2.62}$$

$$\langle E_{kin}\rangle = \int_0^{T_p} \Psi^*(x,t) \frac{p^2}{2m} \Psi(x,t)\, dt \tag{2.63}$$

While $\langle E_{pot}\rangle$ is given by,

$$\langle E_{pot}\rangle = \langle \Psi(x,t)|V|\Psi(x,t)\rangle \tag{2.64}$$

$$\langle E_{pot}\rangle = \left\langle \Psi(x,t) \middle| -\frac{1}{\sqrt{x^2+a^2}} - xE_0 f(t)\sin(\omega t + \phi) \middle| \Psi(x,t) \right\rangle \tag{2.65}$$

Whose integral representation is

$$\langle E_{pot}\rangle = -\int_0^{T_p} \Psi^*(x,t) \left(\frac{1}{\sqrt{x^2+a^2}} + xE_0 f(t)\sin(\omega t + \phi) \right) \Psi(x,t) dt \tag{2.66}$$

2.1.3.2 Dipole acceleration of the atom

The dipole acceleration is a term used to describe the ion - electron motion. The ion (soft core) been massive, remains relatively fixed, while the electron propagates in an oscillatory motion around the ion. This relative motion between the electron and the core is refereed to as the dipole acceleration of the atom. The Ehrenfest theorem in quantum mechanics happens to be the technique commonly used to compute the dipole acceleration [25]. We present in this subsection, a direct and simple way for calculating the dipole acceleration $d_a(t)$.

From the following Hamilton's equation:

$$m\frac{d^2x}{dt^2} = -\frac{\partial H(x,t)}{dx} \tag{2.67}$$

the dipole acceleration takes the form:

$$d_a(t) = -\frac{\partial H(x,t)}{\partial x} \tag{2.68}$$

The expectation value of $d_a(t)$, is given by:

$$\langle d_a(t)\rangle = -\left\langle \Psi(x,t) \middle| \frac{\partial H(x,t)}{d\partial x} \middle| \Psi(x,t) \right\rangle \tag{2.69}$$

The Hamiltonian H is defined as:

$$H(x,t) = T_{\text{ion}} + T_e + V_{\text{at}} + V_{\text{laser}} \tag{2.70}$$

where T_{ion} is the kinectic energy of the soft -core ion, T_e is the kinectic energy of the propagating electron, V_{at} is the soft core atomic potential, V_{laser} is the potential of the laser field.

Now, since the soft-core ion is stationary

$$T_{ion} = 0 \tag{2.71}$$

$$T_e = \frac{P^2}{2m} \tag{2.72}$$

By considering a soft - core hydrogenic system, in $a.u.$, the potential reads:

$$V_{\text{at}} = -\frac{1}{\sqrt{x^2 + a^2}} \tag{2.73}$$

where a is the so-called soft-core parameter.
From Eq.2.7, V_{laser}, is

$$V_{\text{laser}} = -xE(t) \tag{2.74}$$

$$V_{\text{laser}} = -xE_o f(t)\sin(\omega t + \phi) \tag{2.75}$$

Substituting Eq.2.71, Eq.2.72, Eq.2.73 and Eq.2.75 into Eq.2.70, one gets:

$$H(x,t) = \frac{P^2}{2m} - \frac{1}{\sqrt{x^2 + a^2}} - xE_o f(t)\sin(\omega t + \phi) \tag{2.76}$$

With Eq.2.76, it turns out that Eq.2.69 becomes:

$$\langle d_a(t)\rangle = -\left\langle \Psi(x,t)\middle|\frac{d}{dx}\left[\frac{P^2}{2m} - \frac{1}{\sqrt{x^2 + a^2}} - xE_o f(t)\sin(\omega t + \phi)\right]\middle|\Psi(x,t)\right\rangle \tag{2.77}$$

$$\langle d_a(t)\rangle = -\left\langle \Psi(x,t)\middle|\frac{x}{(x^2 + a^2)^2}\middle|\Psi(x,t)\right\rangle + E_o f(t)\sin(\omega t + \phi) \tag{2.78}$$

2.1.3.3 High-order Harmonics Spectrum

From classical physics, we know that an accelerating electron radiates radiation according to Lamor Radiation Law, however, such radiations are not considered for high order harmonic generation, rather it is the emission due to the impulsive acceleration upon recombination that is considered. For the case of our laser field, $E(t)$, the harmonic emission will be brightest in the y-z plane, while there will be zero emission along the x-direction (polarization axis) [17]. As in section (2.1.1), the emitted spectrum is computed from the Frequency Fourier transform of the atomic dipole acceleration.

$$\langle d_a(\omega)\rangle = \mathcal{F}\ [\langle d_a(t)\rangle] \tag{2.79}$$

Using the definition of Frequency Fourier Transform, Eq.2.79 turns out to be;

$$\langle d_a(\omega)\rangle = \frac{1}{\sqrt{2\pi}}\int_0^{T_p} d_a(t)e^{-i\omega t}dt \tag{2.80}$$

$$\langle d_a(\omega)\rangle = -\int_0^{T_p}\left[-\left\langle \Psi(x,t)|\frac{x}{(x^2+a^2)^2}|\Psi(x,t)-\right\rangle\right]e^{-i\omega t}dt + E_o\int_0^{T_p} f(t)\sin(\omega t+\phi)e^{-i\omega t}dt \tag{2.81}$$

It immediately follows that, the HHG spectrum is computed as:

$$S(\omega) = |d_a(\omega)|^2 \tag{2.82}$$

$$S(\omega) = \left|-\int_0^{T_p}\left[-\left\langle \Psi(x,t)|\frac{x}{(x^2+a^2)^2}|\Psi(x,t)-\right\rangle\right]e^{-i\omega t}dt + E_o\int_0^{T_p} f(t)\sin(\omega t+\phi)e^{-i\omega t}dt\right|^2 \tag{2.83}$$

A typical HHG spectrum generated (as shown in Figure 2.7) from direct numerical integration of TDSE was the outcome of using 800 nm, 50 fs with a 5 - cycle pulse laser to interact with an Hydrogen atom.

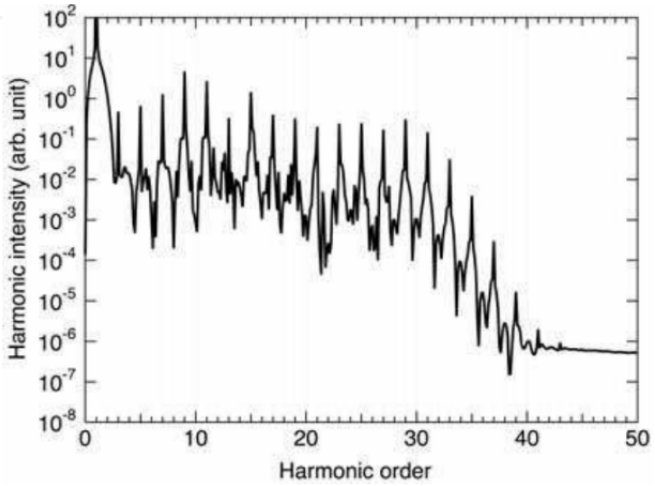

Figure 2.7: HHG spectrum from an H atom[7].

Let's verify the cut-of law in Eq.2.26, by trying to obtain the result shown in the figure above. Then from the equation, the harmonic order N becomes;

$$N = \frac{I_p + 3.17U_p}{w} \tag{2.84}$$

Given $I_p = 0.5\ a.u.$, (see Table 2.2) $I = 2\times 10^{14}W/cm^2$, $\lambda = 800\ nm$, $U_p = \frac{E_o^2}{4\omega^2}$
Recall that we have previously set, $U_p = \frac{E_o^2}{4\omega^2}$. Using Eq. 2.23 ($I = \frac{1}{2}c\epsilon_o E_o^2$) one gets:

$$U_p = \frac{I}{2c\epsilon_o\omega^2} \tag{2.85}$$

where

$$\omega = \frac{2\pi c}{\lambda} \tag{2.86}$$

So, that Eq.(2.85) becomes

$$U_p = \frac{I}{8c\epsilon_o}\left(\frac{\lambda}{\pi c}\right)^2 \tag{2.87}$$

$$U_p = \frac{2\times 10^{18}W/m^2}{8\times 3\times 10^8 m/s\times 8.854\times 10^{12}}\left(\frac{800\times 10^{-9}nm}{\frac{22}{7}\times 3\times 10^8 m/s}\right)^2 \tag{2.88}$$

$$U_p = 1.9095486\times 10^{-18} Joules \tag{2.89}$$

Since 1 $a.u$ of energy is 4.3597×10^{-18} Joules (see Appendix A), U_p now reads, $U_p = 0.438$ $a.u.$. Noting that 1 $a.u.$ of frequency $=4.1341\times 10^{16}s^{-1}$, the highest harmonic order, N of coherent emission is;

$$N = \frac{0.5 + 3.17(0.438)}{0.057} \tag{2.90}$$

$$\therefore N \approx 33 \tag{2.91}$$

This result is in goood agreement with the experimental results in Figure (2.7).

The HHG spectrum plot is usually a semi-logarithmic plot. The vertical axis is the logarithm scale, while the horizontal axis is a real number scale. Two common scaling forms of the horizontal axis are the *Harmonic order* and *Energy* scaling(eV).

(a) Harmonic order (N): In this case, the $a.u.$ of emitted photon frequency ω is divided by the ω_i of the incident photon. i.e.

$$N = \frac{\omega}{\omega_i} \tag{2.92}$$

We adopted the harmonic order horizontal scale in our work.

(b) Energy (eV): In this case, the $a.u$ of emitted photon frequency ω is multiplied by $27.211eV$ (see Appendix A). The conversion between N and eV is defined by;

$$1 \text{ Harmonic order} = \omega_i \times 27.211eV \tag{2.93}$$

In order to estimate the energy range in which the attoseecond pulse in Figure 2.7 were emitted, see Table 2.1. Thus, it follows that, a single attoseconds pulse of 51.18 eV in the soft x-ray region is emitted.

Table 2.1: Energy and wavelength of the Electromagnetic Spectrum

Region	Wavelength (m)	Energy (eV)
Radiowave	> 0.3	$< 7\times10^{-7}$
Microwave	0.001-0.3	7×10^{-7} - 2×10^{-4}
Infra red	7.6×10^{-7} - 0.001	2×10^{-4} - 0.3
Visible	380×10^{-9} - 760×10^{-9}	0.3 - 0.5
Ultraviolet	8×10^{-9} - 3.8×10^{-7}	0.5 - 20
X-rays	6×10^{-12} - 8×10^{-9}	20 - 30,000
γ - rays	$< 6\times10^{-12}$	$> 30{,}000$

2.1.3.4 Characteristics of the HHG Spectrum

Until now, we know that when a laser interacts with an atom, higher energy photons are emitted. Depending on the temporal profile of the driving lasers, the resulting attoseconds pulse could either be a pulse train or single pulse as illustrated in Figure 2.2.

A multiple cycle driving laser results to the generation of attoseconds pulses from each of their half-cycles, thereby resulting to a train of attoseconds pulse, while single cycle driving laser encourages the emission of a single attoseconds pulse [14]. Our interest in this work will be, towards producing a single attosecond pulse. The emitted attosecond pulses can be represented either in time or frequency domain representation.

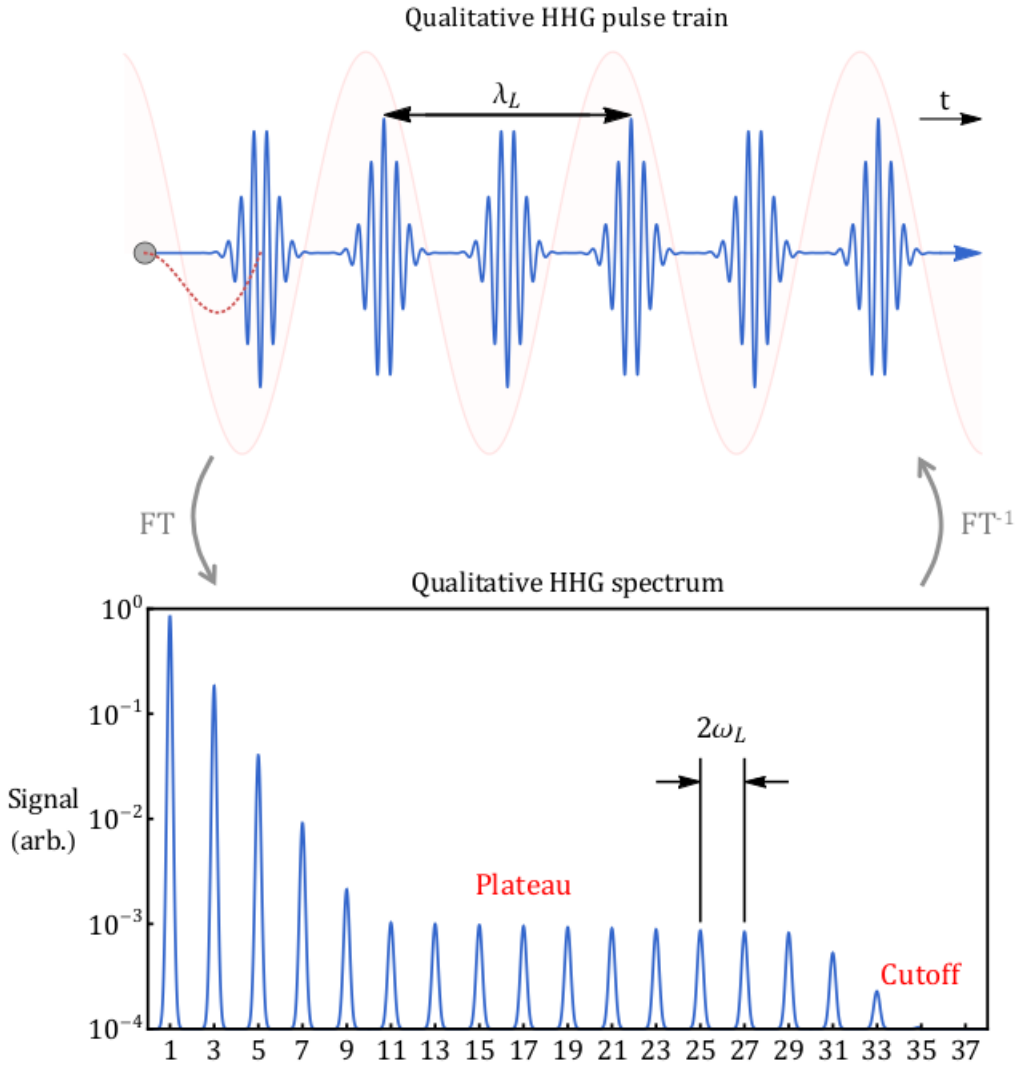

Figure 2.8: Frequency and Time Domain Representation of High order Harmonics[12].

(a) Time domain representation : In order to obtain the time domain $T_{\text{pulse train}}(t)$ representation, we perform an inverse Fourier Transform[4] of Eq.2.83 [8], as per:

$$T_{\text{pulse train}}(t) = \mathcal{F}^{-}|S(\omega)| \tag{2.94}$$

[4]Note that Eq.2.83 and Figure 2.7 represent the frequency domain representation of the attoseconds pulses.

$$I_{\text{pulse train}}(t) = \left| \frac{1}{\sqrt{2\pi}} \int_0^{T_p} S(\omega) e^{i\omega t} d\omega \right| \tag{2.95}$$

If it is required to obtain the time domain characteristics of an isolated attoseconds pulses $T_{\text{singe pulse}}(t)$ then we perform the inverse Fourier Transform only across the length of the plateau region[8].

Let $q = q_2 - q_1$ (the number of harmonics spanning the plateau length); t_1 and t_2 the time corresponding to q_1 and $t_2$respectively. It turns out that:

$$I_{\text{singe pulse}}(t) = \left| \frac{1}{\sqrt{2\pi}} \int_{t_1}^{t_2} S(\omega) e^{i\omega q t} dt \right|^2 \tag{2.96}$$

Figure 2.9 represents a pictorial illustration of time domain of an HHG.

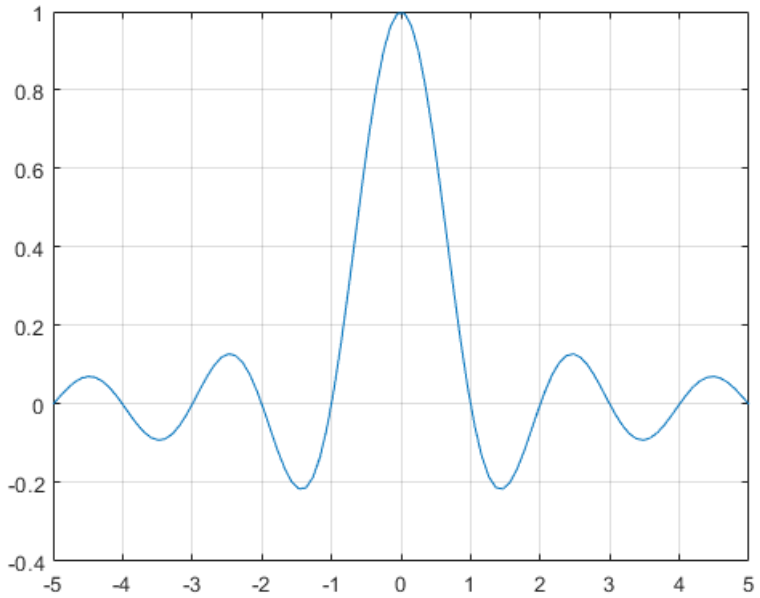

Figure 2.9: Temporal profile a single attosecconds pulse [23].

(b) Frequency (Spectrum) domain representation: The Frequency Fourier transform of the time domain attoseconds pulse gives the spectrum representation. Figure 2.8 shows the conversion scheme between the spectral and temporal HHG representation. By this simple action, details in the emitted photon can be extracted. It is a plot of Intensity [5], S(arbitary unit) as function of photon energy ω. A typical HHG spectrum of the type in Figure 2.8 has 3 distinct regions, namely; *perturbative region*, *plateau region* and *cut-off region* [25].

(i) Perturbative region: This region is characterized by a rapidly decreasing yield with increasing harmonic order. This behaviour can be understood by considering an atom absorbing n photons then emitting a single photon. The probability of absorbing n photons decreases as n increases, explaining the rapid decreases in the initial intensities [3].

[5]The Intensity has an arbitrary unit

(ii) Plateau region: In this region, the number of absorbed photons remains constant; i.e a saturation will occur. As such, a flat and broad region in the spectrum will be seen. In this region, all the harmonics are coherently emitted (have approximately the same intensity in phase). Plateau harmonics spanning several tens of harmonic order have been measured which extends into the soft-xray regime [14].
The observed saturation intensity depends on the noble gases used. Gases with lower I_p leads to higher intensity of the generated pulses. Typically the region that begins the plateau is I_p[14]. The width of each spectral peak in this region, is referred to as bandwidth w. The spectral banwidth w is related to the pulse width τ by the relationship;

$$\tau = \frac{1}{w} \tag{2.97}$$

The larger the spectral width, the smaller the value of τ. This implies that broader plateau are produced by shorter attoseconds pulses. In the next section we will see that broader plateau region supports single attoseconds pulse generation [14].

(iii) Cut-off region: This marks an abrupt end of the pleateu region. It gives a measure of the maximum energy of the emitted attoseconds pulse [17]. From Eq.2.25 and Eq.2.85, the cut-off energy varies linearly with the laser intensity I, and Ionization potential I_p. As illustrated in Table 2.2, I_p is dependent on the gases used as the atomic target.

Table 2.2: Ionization Energies of Noble Gases[13].

	Ionization energy (I_p)	
Atomic species	eV	$a.u.$
H	13.6	0.5
He	24.587	0.904
Ne	21.565	0.79
Ar	15.759	0.58
Kr	13.999	0.51
Xe	12.129	0.45

Higher I extends the cut-off as well as higher I_p. A gase that supports higher cut-off energy leads to reduced saturation intensity of their plateau region. He and Ne would have been the best candidates for for higher energies, but their intensities will be compromised. So, there is a balance to be found depending on the intensity and energy of the expected attosecods pulse [14]. Our interest in this work will be on maximizing the highest obtainable energy. Therefore we shall use the Hydrogen atom as our atomic species.

CHAPTER 3

SINGLE ATTOSECOND PULSE

3.1 Fundamentals of Single Attoseconds Pulse

We have already seen in the previous section that a multi-cycle incident laser is capable of generating a train of attosecond (as) pulse. If one, however, decides to obtain a single pulse, then the number of cycles in the incident laser needs to be reduced [9]. We can have fewer cycles experimentally, by chirping. Laser pulse chirping is a technique employed to produce a single cycle pulsed laser by chopping-off the side peaks and leaving behind the central peak in the pulse envelope. We shall however seek to bypass experimental requirements for generating this ultrashort incident pulses, by considering the interaction of two femtosecond laser pulses. When the parameters of these driving lasers are carefully selected, a nearly single-cycle pulsed laser can be achieved from their interaction.

In our work, and as what is obtainable in most literatures, we shall apply the two-colour scheme. This involves coupling a second laser source to the incident 800 nm Ti: Sapphire laser. As a common nomenclature, the 800 nm Ti: Sapphire laser is called *the fundamental laser*, and the second laser as *the secondary laser*. In literatures, the secondary laser used where either high harmonics of the fundamental laser field or an arbitrary laser field. A secondary laser field of a lower wavelength has a constructive interference at the second or third peak when mixed with the fundamental field. This unfortunately does not favour the generation of a broader plateau. Hence a secondary laser field of a higher wavelength and higher number of cycles are often preferred [9]. We shall however demonstrate a counter opinion, in which we have generated higher energy attosecond pulses by using a secondary laser field of lower wavelength (400 nm). With these new configurations, the resultant form (synthesized laser) of the driving laser shows marked differences [9]. Figure 3.1 shows an example of a fundamental laser (green), secondary laser (red) and synthesized laser (blue).

The addition of the secondary field is observed to divide the electric field profile of the fundamental pulse into three segments, namely the first, the middle and last segments. The electric field amplitude of the first and last segments are dramatically suppressed in relation to the middle segment. Thus, it is realized that, the mixture of different colour can result in a larger difference in the field amplitude among neighbouring cycles than in a single color field [9].

If this synthesized pulse is adopted as the incident driving pulse, only the middle segment of the electric field makes a major contribution to the plateau and the cut - off position of the harmonic spectrum. The electric field of this specific two-color pulse is similar to that of an isolated 5 fs ultrashort pulse, but it relaxes the requirements for the pump pulse duration. That is to say, we may obtain an isolated attosecond pulse under the frame of a multicycle two-color driving pulse [12]. Broadly speaking, three (3) gating

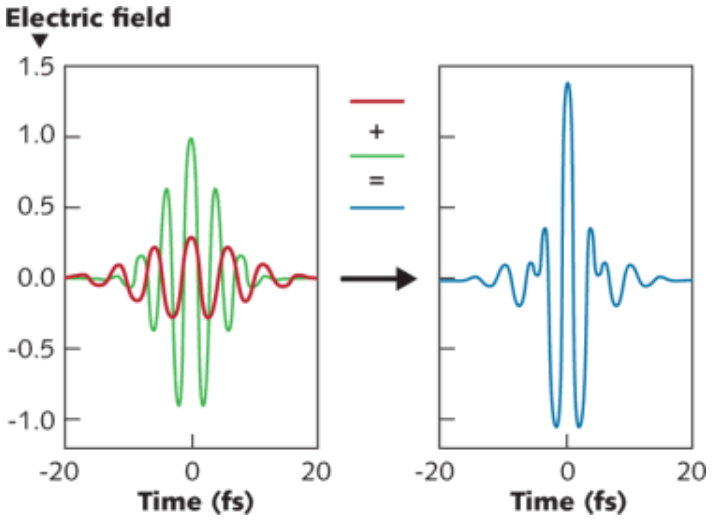

Figure 3.1: Two color mixing of an incident laser. Green: fundamental field, Red: secondary field, Blue: synthesized field [8].

schemes are used to produce an isolated attoseconds pulse. They are temporal gating, spatial gating and spatio-temporal gating [14]. A temporal gating is the technique that has been discussed so far. The other two schemes will not be captured in this work.

The essential properties of a typical *synthesized laser* can be summarized as per:

(i) Short time duration

(ii) Few cycles within a pulse

(iii) Large amplitude difference between the strongest and 2^{nd} strongest cycle in the synthesized laser.

It has been demonstrated that the broadness of the plateau is dependent on the amplitude difference between the strongest and 2^{nd} strongest cycle in the synthesized pulse [9]. A parameter referred to as the intensity ratio difference, δ_d was used as a deterministic factor for plateau length, defined as per:

$$\delta_d = \frac{E_1^2 - E_2^2}{E_1^2} \tag{3.1}$$

where E_1^2 and E_2^2 represent the strongest and the second strongest amplitude of the cycles respectively. From Eq.(1.24) and Eq.(2.26). It turns out that the larger the field amplitude, the higher the cut-off energy of the harmonic photons. So, that larger amplitude differences of $E_1^2 - E_2^2$, results to wider plateau. In their simulation studies, they plotted δ_d and plateau length (otherwise called continuum length) against wavelength, in order to determine the optimum wavelength of the needed secondary laser field. It was observed that δ_d increases with the continuum length upto a certain maximum and vice-versa.

One important implication of a broad plateau is the ease of isolation of a single pulse. The several peaks in the plateau region represents some n- number of coherent pulses stacked together. Broader plateau implies that the corresponding time domain of each peak is ultrashort [12]. Figure 3.2 shows the pulse repetition rate of a short and ultrashort attosecond pulse.

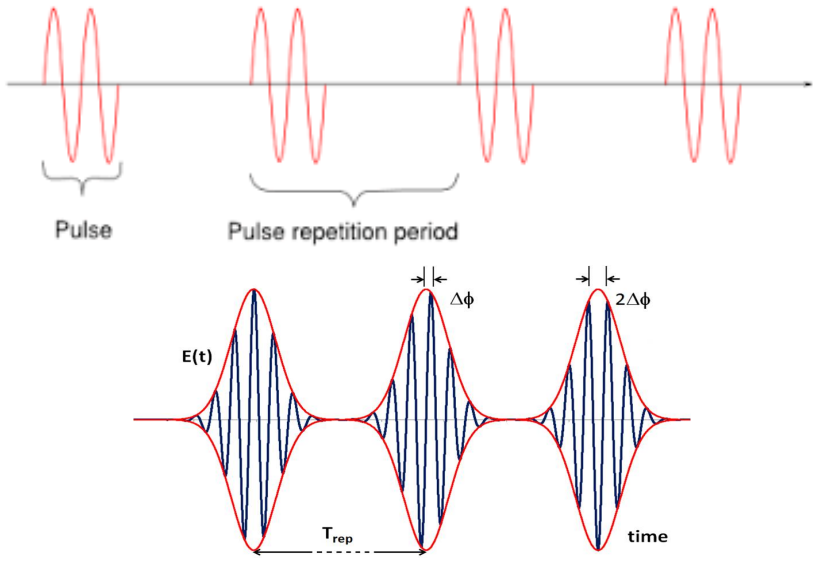

Figure 3.2: The effect of pulse repetition rate, T_{rep} on easy attoseconds pulse isolation[7].

As seen in the Figure 3.2, ultrashort pulses defined by fewer cycles have a larger pulse repetition rate, T_{rep} hence they can easily be selected because they are widely spaced. Though, the two-color mixing technology are excellent for producing higher energy cut - off, but the intensity of the photons are generally low [8]. Hence, the optimization of the two-color scheme for practical applications is important. Remarkably, the intensity $I(t)$, and phase ϕ variation as well as time lag between the two laser fields τ have been studied [8, 9, 6]. We shall endeavour to review recent works in these regard.

3.2 Temporal Gating (two color mixing)

In this section, we aim to summarize a handful of literature works that employed the two color mixing techniques.

3.2.1 Two Intensity Mixing

A simulation studies was carried out on an Helium atom by [9] for which, two colours were mixed together, with the aim of optimizing the intensity. The Lewestein Model was employed to generate the HHG spectrum of which 800 nm Ti: Sapphire laser was used throughout, as the fundamental field. The equation for the form of the linearly polarized synthesized laser field can be expressed as follows:

$$E(t) = E_1 e^{-2ln2\frac{t^2}{\tau_1^2}} \cos(\omega_1 t) + E_2 e^{-2ln2\frac{t^2}{\tau_2^2}} \cos(\omega_2 t) \tag{3.2}$$

where E_1, τ_1 and ω_1 are the field amplitude, FWHM and frequency of the fundamental laser respectively. Likewise, E_2, τ_2 and ω_2 are the field amplitude, FWHM, frequency of the secondary laser respectively.

Table 3.1 below summarizes the optimization result of the simulation. The second column represents the information of the single as, and plateau extension. The first and last columns define the parametrics (λ, τ_1, $I(t)$) of the laser. Here, E_1, E_2 and ω_1, ω_2 can be calculated using Eq.(2.23), Eq.(3.89) respectively. Throughout, indices 1 and 2 stand for the fundamental laser and secondary laser respectively.

Table 3.1: Driving lasers parameters and HHG results

	Fundamental laser	as/-plateau extension	Secondary laser
i	800 nm, 6fs, 3 $\times 10^{14}$ W/cm^2	90 as	1760 nm, 64fs, 1.1 $\times 10^{14}$ W/cm^2
ii	800 nm, 11fs, 3 $\times 10^{14}$ W/cm^2	80 as (160 - 260 eV)	1840 nm, 64fs, 1.1 $\times 10^{14}$ W/cm^2
iii	800 nm, 11fs, 5 $\times 10^{14}$ W/cm^2	80 as (160 - 260 eV)	1440 nm, 64fs, 1.1 $\times 10^{14}$ W/cm^2
iv	800 nm, 22fs, 3 $\times 10^{14}$ W/cm^2	180 as	1840 nm, 64fs, 7.5 $\times 10^{14}$ W/cm^2
v	800 nm, 33fs, 5 $\times 10^{14}$ W/cm^2	230 as	1840 nm, 64fs, 2.9 $\times 10^{13}$ W/cm^2

Three frequency forms (1440 nm, 1760 nm, and 1840 nm) of the secondary lasers were used to interfere with the fundamental laser. Characteristics (ii) and (iii) are the most favourable for single as. Note that 80 as with a broad pleateun extending from 160 to 260 eV were obtained with higher intensities of the fundamental laser than the secondary laser.

3.2.2 Two Phase Mixing

A Numerical Simulation of an Intense Isolated Attosecond Pulse by a Chirped Two-Color Laser Field was recently carried out [8]. The work involved a direct simulation of the TDSE for He atom using the split operator method. An isolated 126 as pulse with maximum harmonic order N of 450 was observed. This was achieved using the fundamental laser (800 nm, $10^{15} W/cm^2$) assisted with the secondary laser (1600 nm, 10 fs) and by varying the FWHM of the fundamental laser and the intensity of the secondary laser.The equation defining the synthesized pulses is given by:

$$E(t) = E_1 f_1(t)\cos(\omega_1 t + \delta(t)) + E_2 f_2(t)\cos(\omega_2 t) \tag{3.3}$$

Where $\delta(t) = -\beta \tanh \frac{t}{\sigma}, \quad \omega_1 \rightarrow \omega_1 + \frac{d\Delta(t)}{dt} = \omega_1 - \frac{\beta}{\sigma}\cosh^{-2}(\frac{t}{\sigma})$

$E_i, \quad f_i(t) = e^{-4ln2\frac{t^2}{\tau_i^2}}, \quad \omega_i \quad \text{for}, i = 1, 2$

Here, $\delta(t)$ is the phase. β (which controls the frequency sweeping range of the fundamental pulse) and σ (which controls the chirping steepness of the fundamental pulse) are varied, thereby affecting $\delta(t)$ and ω_1. The simultaneous variation of $\Delta(t)$ and ω_1 ultimately results to chirping.

The simulation was specifically carried out with the following laser parameters as per:

(i) σ and β were set to zero. This is the simplest case for the two-color scheme (without chirping). The laser parameters are
Laser 1: 7fs, 800 nm, $10^{15} W/cm^2$
Laser 2: 10fs, 1600 nm, $10^{14} W/cm^2$

(ii) σ was fixed at 200 $a.u$ while β was varied. The optimum value of β corresponding to the highest cut-off was 6.25. The laser parameters are
Laser 1: 7fs, 800 nm, $10^{15} W/cm^2$
Laser 2: 10fs, 1600 nm, $10^{14} W/cm^2$

(iii) For σ was fixed at 200 and β at 6.25, while the intensity of the secondary laser was varied. The laser parameters are
Laser 1: $7fs$, 800 nm, $10^{15}W/cm^2$
Laser 2: $10fs$, 1600 nm, $10^{15}W/cm^2$

It turns out that the optimum result corresponds to case (iii) for which a single pulse duration of 126 as of 450 harmonic order were observed.

3.2.3 Time Lag

The time lag/delay refers to a shift in time between when a fundamental and a secondary fields. A time delay could either be positive or negative. A positive time delay means that the pulse envelope (of the secondary field) comes before that of the fundamental field, and vice versa. There are two aspects of time lag consideration which are;

- The time lag between multi-cycle fields: Here, the time lag is equivalent to Carrier Envelope Phase, ϕ. Assuming a positive time delay between two laser fields containing multi cycles, the associated synthesized field can be written as:

$$E(t) = E_1 f_1(t)\cos(\omega_1 t) + E_2 f_2(t+\tau)\cos(\omega_2 t + \phi) \tag{3.4}$$

  τ is time delay. More generally (3.4) can be redefined as

$$E(t) = E_1 f_1(t)\cos(\omega_1 t) + E_2 f_2(t+\tau)\cos[\omega_2(t + \phi/\omega_2)] \tag{3.5}$$

  where

$$\tau = \phi/\omega_2 \tag{3.6}$$

- The time lag between few cycle fields: When short pulses containing few oscillations are considered, a time delay between two pulses envelope can no longer be viewed as equivalent to a CEP shift. Consider the sine carrier form of synthesized laser without time delay, $E_{ntd}(t)$

$$E_{ntd}(t) = E_1 f_1(t)\sin(\omega_1 t + \phi_1) + E_2 f_2(t)\sin(\omega_2 t + \phi_2) \tag{3.7}$$

A theoretical and simulation studies were carried on H atom [6]. They adopted the direct simulation of the TDSE, expressed in spherical coordinates, and which was solved using a time-dependent generalized pseudo-spectral method, upon which the wavefunction is expanded in Legendre polynomials and the time propagation done with a second-order split operator technique. And because this model is not quite informative, their results were analysed and interpreted using time -frequency and analytical analysis.

A 800 nm fundamental laser field was assisted with their second harmonic ω_2 $(= 2\omega_1)$ and third harmonic ω_3 $(= 3\omega_1)$. Both fields contained few cycles. The FWHM τ and intensity I of the fields were fixed at (fundamental: $8.0fs$, $6 \times 10^{13}W/cm^2$) and (secondary: $5.6fs$, $4 \times 10^{13}W/cm^2$) respectively.
The simulation procedure can be divided into 4 stages. As we shall shortly see, stage i-iii major on positive time delay, while the remainder is centered on comparing positive and negative time delay.
In all of these procedures, the parameters that varied other than the frequency of the

secondary lasers are ϕ_1 and ϕ_2. Since τ is dependent on ϕ_2. It implies that as ϕ_2 is varied, τ also varies.

The simulation was carried out with the following laser parameters per as:

(i) Firstly, ϕ_2 is varied while ϕ_1 and $\phi_2^{'}$ are set to 0. In this two colour mixing technique, the second harmonics ω_2 is used. Two spectrum are obtained, one without time delay and another with time delay. It was shown that the time delay case was favourable to the generation of attosecond pulse of high intensity, but having a low cut-off energy.

(ii) Here, both ϕ_1 and ϕ_2 are varied. Again, two spectra, without and with time delay were obtained. In a much similar situation as above, high intensity attosecond pulse with loow cut-off energy was obtained.

(iii) Also, the same form of the spectral is realized when ϕ_2 is varied in conjunction with/without ϕ_1 and $\phi_2^{'}$.

(iv) Furthermore, the above procedures were repeated, only that a negative time delay was considered. Results from the respective spectra indicated a better intensity yield over the cut-off energy. However, no emphasis was placed in generating an isolated attosecond pulse.

CHAPTER 4

SIMULATION PROCEDURE

This chapter presents the methodology of the research, in systematic arrangement of how the simulation is been carried out on the computer. Firstly, we define the environment of the simulation work, referred to as the grid and absorber system. Within the environment, we setup a system that mimics the H atom, and hereafter, a laser beam was introduced to interact with the H atom. Upon irradiation, the Hydrogen electron oscillates within the simulation environment back and forth the H core. Measurement of the electron motion and its total energy due to propagation was done, including the attosecond pulse arising from the re-collision of the H electron with its core.

4.1 Grid and Absorber System

The grid was the environment of the simulation accommodating the motion of the electron. It consist of the position, momentum and time grid. The position grid was defined large enough to contain the propagation and recombination motion of the electron. Its length, L was

$$L = 2\pi L_x \tag{4.1}$$

where L_x is an arbitrary number, used to control the length of the grid. The momentum grid was defined based on the specifications of the position grid, while the time grid was defined independently of either the position or momentum grid. The absorber system was defined on the position grid and serves as a form of restraint to the electron motion.

4.1.1 Position Grid

The position grid has a size of $\left[-\frac{L}{2}, \frac{L}{2}\right]$ Each point x_m in the grid has the relation;

$$x_m = x_{min} + m\Delta x \tag{4.2}$$

Where $\Delta x = \frac{x_{max} - x_{min}}{N_x}$, $m = 0, ..., N_x - 1$, $x_{max} = \frac{L}{2}$, $x_{min} = -\frac{L}{2}$, N_x is the number of position grid points. Δx is the position step size. See Appendix B for the specifications of the position grids.

4.1.2 Momentum Grid

The momentum grid has a size of $[-p_{max}, p_{max}]$. Each point p_m in the grid has the relation;

$$p_m = p_{min} + m\Delta p \tag{4.3}$$

where Δp is momentum step size. $p_{max} = \frac{\pi}{\Delta x}$

$$\Delta p = \frac{p_{max} - (-p_{max})}{N_x} = \frac{2\pi}{N_x \Delta x} \tag{4.4}$$

Therefore, setting $p_{min} = 0$, Eq.4.3 becomes

$$p_m = m\left(\frac{2\pi}{N_x}\right)\left(\frac{N_x}{2\pi L_x}\right) \tag{4.5}$$

$$p_m = i\left(\frac{1}{L_x}\right) \tag{4.6}$$

Δt is the step size. See Appendix B for the specifications of the momentum grids.

4.1.3 Time Grid

Different time grid was used for the imaginary propagation, real propagation and spectrum computation, depending on the values corresponding to the expected results. The step size were however chosen very small in accordance to Baker Campbell Approximation.

The time grid had a size of $[0,\ t_{max}]$. Each point t in the grid has the relation;

$$t = t_0 + m\Delta t \tag{4.7}$$

where

$$\Delta t = -i\left(\frac{t_{max}}{N_t}\right) \tag{4.8}$$

$t_0 = 0,\ \ m = 0, ..., N_t - 1,\ \ t_{max}$ is the maximum time, N_t is the no of points in the time grid, Δt is the time step. See Appendix B for the specifications of the imaginary, real and spectrum time grids.

4.1.4 Boundary Absorber

A boundary absorber is a potential, added to the laser potential to cause a damping action on the electron motion near the grid boundaries. The form of the absorber used in our work, was the optical potential. Potential ofthis kind are purely imaginary absorber that operates to weaken the strength of the electron density as it approaches the two edges in the grid [11].

$$V_{opt} = -i\left[\theta(x - x_1)\left(\frac{x - x_1}{x_{max} - x_1}\right)^2 - \theta(x_2 - x)\left(\frac{x - x_2}{x_{min} + x_2}\right)^2\right] \tag{4.9}$$

Where $x_1 = x_{max} - \frac{5\pi L_x}{10}$, $x_2 = x_{min} + \frac{5\pi L_x}{10}$, θ is the step function, which controls the absorption. The form of absorber used for the single color lasers is as shown in Figure 4.1, while Figure 4.1b is the corresponding absorber for the the two color laser field.

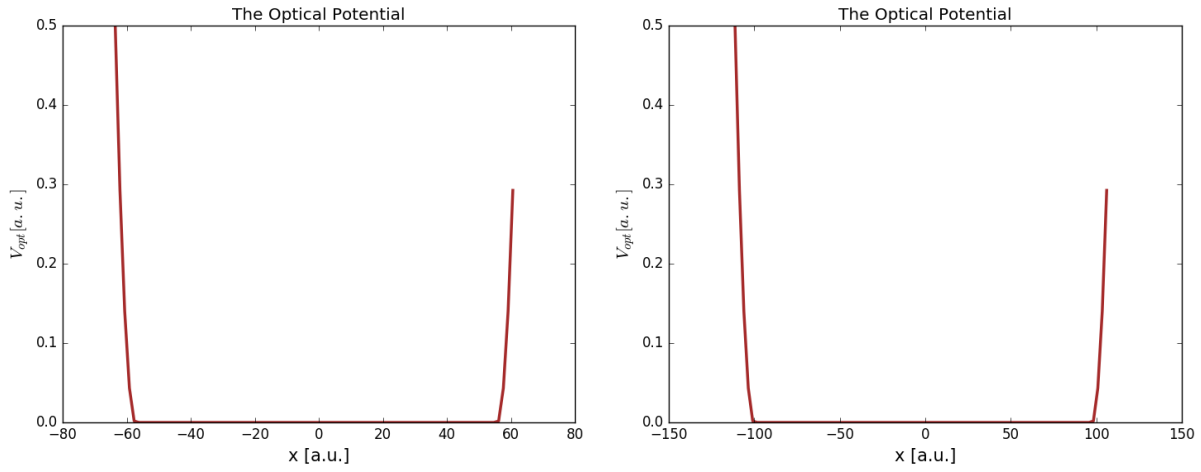

(a) (b)

Figure 4.1: Absorber Potential

The maximum strength of V_{opt}, is 0.5. However if $V_{opt} = 1.0$ (same as the strength of the wavepacket $[\psi]^2 = 1$), then it behaves in similar way as the grid boundaries. In such cases, the wavepacket are heavily reflected[1] at x_1 and x_2 thereby resulting to entrance of ghost wavefunction and eventually leading to spurious harmonics.

By defination V_{opt} acts at region x_1 (-60 and -100) and x_2 (60 and 100). An electron wavepacket approaching x_1 from the origin becomes moderately absorbed at x_1. And as it makes further translation from x_1 to x_{min}, the remainder of $[\psi]^2$ were all absorbed. So, that at the edge (x_{min}) there was practically no wavepacket. Thus the possibility of a ghost wavefunction entering our system was prevented. Similar action also took place between x_{max} and x_2 when the wavepacket advanced toward the right edge of the grid.

4.2 Setting up the Atomic System

4.2.1 Soft Core Potential

The core potential of the H atom is

$$V = -\frac{e}{4\pi\epsilon_o x} \tag{4.10}$$

in a.u. Eq.4.10 becomes

$$V = -\frac{1}{x} \tag{4.11}$$

However in order to avoid singularity when $x = 0$, and to allow the electron motion to continue along x, the core potential is softened so that;

$$V_{\text{soft core}} = -\frac{1}{\sqrt{x^2 + a^2}} \tag{4.12}$$

Refer to Figure 4.2 for the form of potentials. The value of 'a' has an effect on the broadness of the plateau. It has been verified that, smaller values of a gives rise to broader plateau than larger values [13]. The Soft-core potential was centered at the position grid. See Appendix B for the chosen values of a both for the single and two color simulation.

[1]The occurrence of wavepacket reflection at the grid boundaries was because the evolving wavepacket must be periodic, according to the FFT action in propagating the wavefunction

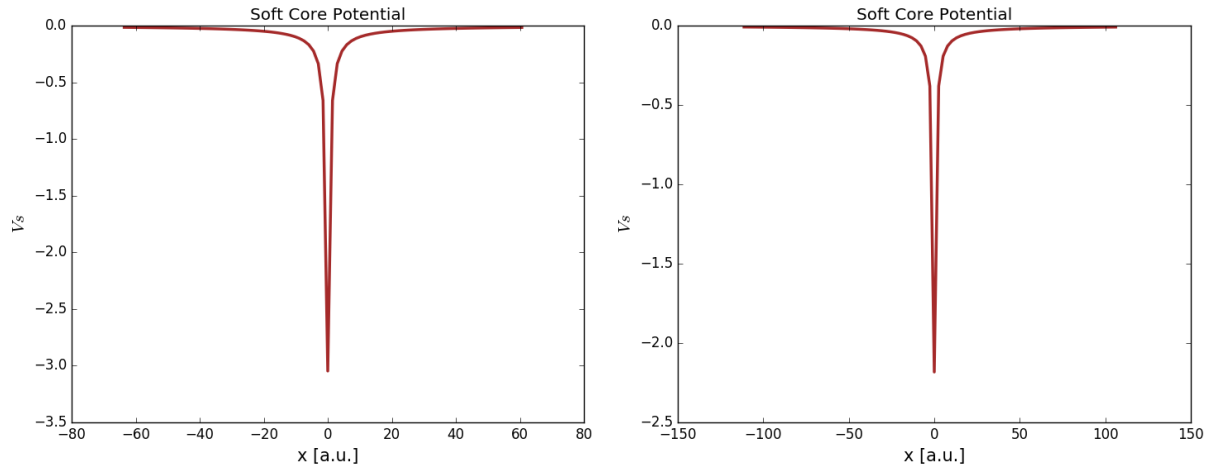

(a): for single color case (b):for double color case

Figure 4.2: Soft Core Potential

As seen in Figure 4.2a and Figure 4.2b, the depth of the potential well differs as a result of different values of a. The nuclei is located at the bottom of the core, while the electron is situated above the core.

4.2.2 Imaginary Time Propagation

We adopted an initial wavefunction $\psi(x, 0)$, given by;

$$\psi(x, 0) = e^{-\frac{x^2}{2}} \tag{4.13}$$

The absorber was added to the soft-core potential. So, we have a modified potential of the form;

$$V \rightarrow V_{\text{soft core}} + V_{abs} \tag{4.14}$$

We performed an imaginary time action (i.e going back in time) so.

$$\Delta t \rightarrow -i\Delta t \tag{4.15}$$

It turns out that Eq.2.54 becomes

$$\Psi(x, t_0 + \Delta t) = e^{-\frac{1}{2\hbar}(V_{\text{soft core}}+V_{abs})\Delta t}.e^{-\frac{1}{\hbar}T\Delta t}.e^{-\frac{1}{2\hbar}(V_{\text{soft core}}+V_{abs})\Delta t}e^{-\frac{x^2}{2}} \tag{4.16}$$

Where $t_0 = 0$. The actions in Eq.2.55 to Eq.2.60 were carried out, to get the final form of $\Psi(x, t_0 + \Delta t)$ denoted as $\Psi_{img}(x, t)$

The initial and imaginary propagated electron density are depicted in Figure 4.3

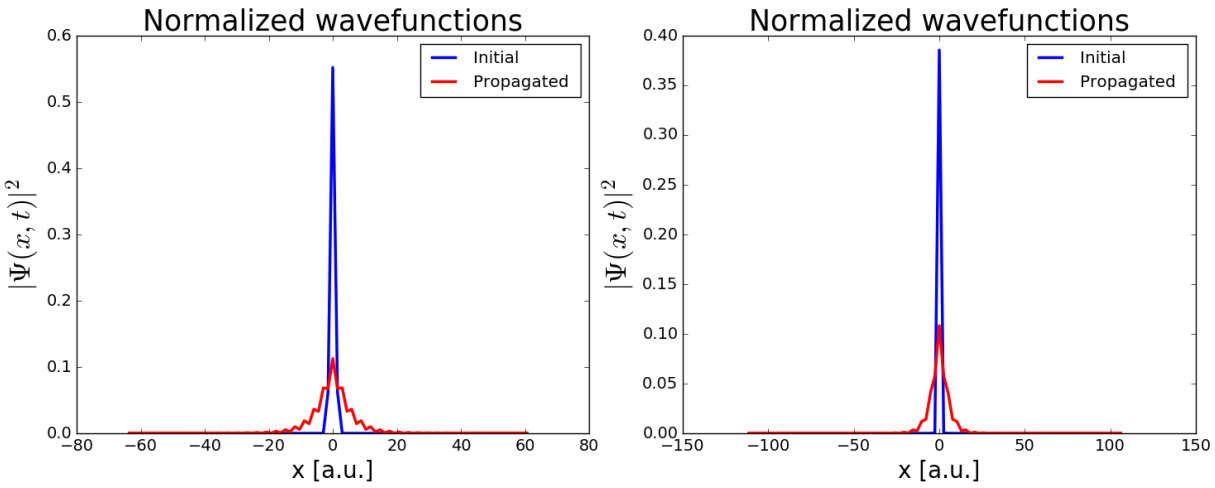

(a): for single color case

(b):for double color case

Figure 4.3: Electron probability distribution

For the colour code in Figure 4.3, BLUE represented the initial wavefunction, while RED represented the ground state wavefunction. In Figure 4.3a, the electron was initially located at the origin with a probability of 0.55, but after relaxing the system through imaginary time propagation, the probability dropped to 0.1, same as that obtained with the two color laser. In Figure 4.3b, the electron was initially closer to the origin than in (a), so the time for relaxation was typically smaller (see Figure 4.3).

4.2.3 Computation of the Ionization-energy Observable

We computed the the energy of the H electron by using Eq.2.63 and Eq.2.66. Thus

$$\langle E_{kin} \rangle = -i \sum_{0}^{t_{max}} \Psi^*_{img}(x,t) \frac{p^2}{2m} \Psi_{img}(x,t) \Delta t \tag{4.17}$$

while $\langle E_{pot} \rangle$ is given by;

$$\langle E_{pot} \rangle = -i \sum_{0}^{t_{max}} \Psi^*_{img}(x,t)(V_{\text{soft core}} + V_{abs}) \Psi_{img}(x,t) \Delta t \tag{4.18}$$

The ionization-energy, I_p now reads;

$$I_p = \langle E_{kin} \rangle + \langle E_{pot} \rangle \tag{4.19}$$

I_p now represents the total energy of the electron in Figure 4.4. The energy plot shown in the Figure reveals that the atomic species was an H atom.

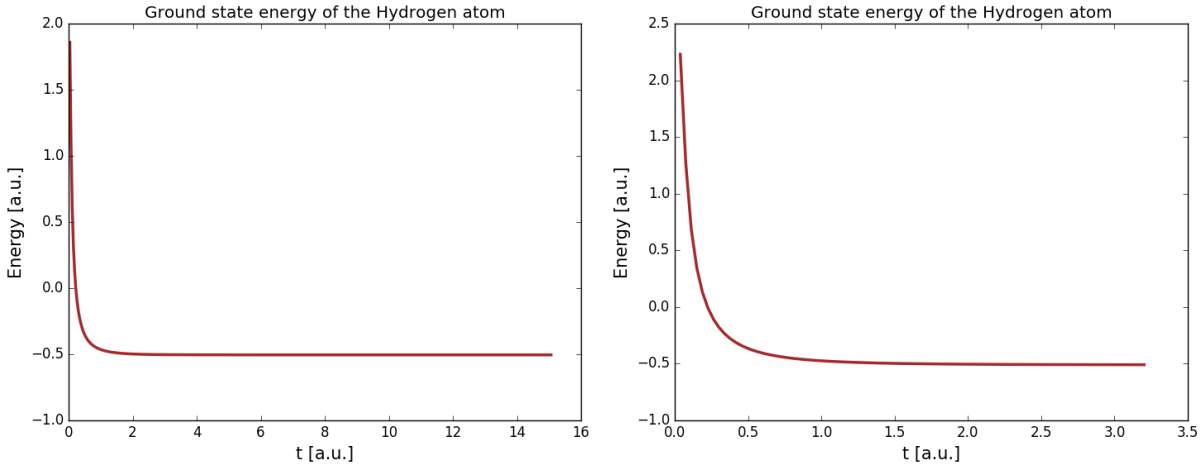

(a): Energy relaxation for single color (b):Energy relaxation for double color

Figure 4.4: Ground state energy plot for H atom

In Figure 4.4a, the electron's initial energy was approximately 1.8 $a.u.$, but after about 2 $a.u.$ time of propagation the system was well relaxed. In Figure 4.4b, the electron's initial energy was approximately 2.25 $a.u.$, but after about 1.5 $a.u.$ time of propagation the system was well relaxed. The reason for the shorter relaxation time was due to the fact that the electron was initially located close to the grid origin, as such minimum time is required for its relaxation even though its initially energy was higher than in Figure 4.4a.

4.3 Laser Irradiation

Two forms of laser fundamental fields were separately coupled to the H atom. The forms of the fundamental and secondary field were already given (see Eq.1.17), and refer to Eq.4.20 for the form of the synthesized field.

$$E(t) = E_1 f_1(t)\sin(\omega_1 t) + E_2 f_2(t+\tau)\sin[\omega_2(t+\tau)] \tag{4.20}$$

Where $\tau = \frac{\phi}{\omega_2}$. The laser parameters are given in Table 4.1.

Table 4.1: Incident laser parameters

	Wavelength (λ) nm	intensity $(10^{14})W/cm^2$	n_c
1^{st} fundamental	800	2	10
2^{nd} fundamental	800	4	10
secondary	400	5	20

The chosen parameters of τ and ϕ are given in Table 4.2

Table 4.2: Incident time lag parameters

	τ ($\frac{\phi}{\omega}$) a.u.	ϕ
(i)	50	0.04π
(ii)	400	0.2π
(iii)	1768	π
(iv)	3203	1.6π

4.3.1 Soft Core-Laser Potential

The total potential of the system (otherwise called soft core-laser potential) was computed as a sum of Eq.2.6, Eq.4.9 and Eq.4.12. i.e

$$V = V_{\text{soft core}} + V_{laser} + V_{opt} \tag{4.21}$$

4.3.2 Real Time Propagation

We performed real time propagation by setting

$$\Delta t \rightarrow \Delta t_{real} \tag{4.22}$$

It turns out that Eq.2.54 becomes;

$$\Psi(x, t + \Delta t_{real}) = e^{-\frac{1}{2\hbar}V\Delta t_{real}}.e^{-\frac{1}{\hbar}T\Delta t_{real}}.e^{-\frac{1}{2\hbar}V\Delta t_{real}}\Psi_{img}(x,t) \tag{4.23}$$

The actions in Eq.2.55 to Eq.2.60 were carried out, to get the final forms of $\Psi(x, t+\Delta t_{real})$ denoted as Ψ_{real}

4.3.3 Computation of the Accelerating electron's -energy

During the propagation motion of the electron under the influence of the laser field, the maximum attainable energy which we have earlier refereed to as the ponderomotive energy U_p, was computed by th foloowing expression using Eq.2.63 and Eq.2.66.

$$\langle E_{kin}\rangle = \sum_{0}^{t_{max}} \Psi^*_{real}(x,t)\frac{p^2}{2m}\Psi_{real}(x,t)\Delta t_{real} \tag{4.24}$$

$$\langle E_{pot}\rangle = \sum_{0}^{t_{max}} \Psi^*_{real}(x,t)V\Psi_{real}(x,t)\Delta t_{real} \tag{4.25}$$

$$E_{total} = U_p = \langle E_{kin}\rangle + \langle E_{pot}\rangle \tag{4.26}$$

4.4 Spectrum Generation

By using Eq.2.83, we simulated the spectrum $S(\omega)$ as;

$$S^1(\omega) = \left| \frac{1}{\sqrt{2\pi}} \sum_{0}^{t_{max}} \left(\sum_{0}^{t_{max}} \Psi^*_{real}(x,t) \frac{x}{(x^2+a^2)^{3/2}} \Psi_{real}(x,t) \Delta t_{real} - E(t) \right) e^{-i\omega t} \Delta t_{spec} \right|^2 \tag{4.27}$$

where Δt_{spec} is the time step in the spectrum time grid.

4.5 Single Pulse Generation

An inverse fourier transform of the frequency spectrum can be performed to get the corresponding single temporal pulse.

For the single attoseconds pulse due to the field $E(t)$, we have;

$$S^{-1}(\omega) = \mathcal{F}^-|S(\omega)| = \frac{1}{\sqrt{2\pi}} \sum_{t_1^1}^{t_2^1} S^1(\omega) e^{i(q_2^1 - q_1^1)\omega t} \Delta t_{spec} \tag{4.28}$$

where $q_2^1 - q_1^1$ = harmonic order in the plateau region ; t_2^1, t_1^1 are the corresponding time The above however is a common technique for visualizing a single attoseconds pulse.

ALTERNATIVELY;

We decided to generate the single attoseconds pulse from the computed dipole acceleration. By using Eq.2.78, we simulated $d_a(t)$ as;

$$d_a(t) = \sum_{0}^{t_{max}} \Psi^*_{real}(x,t) \frac{x}{(x^2+a^2)^{3/2}} \Psi_{real}(x,t) \Delta t_{real} - E(t) \tag{4.29}$$

Observe from the Hamilton's equation, that the dipole acceleration is a direct representation of the electric field profile of the generated attoseconds pulse.

$$m\frac{d^2x}{dt^2} = -\frac{dH}{dt} = -eE(t) \tag{4.30}$$

By considering $a.u.$ conversion (See Appendix A), we obtain;

$$d_a(t) = \frac{d^2x}{dt^2} = -E(t) \tag{4.31}$$

By making use of the conversion;

$$1\text{a.u. of time} = 2.4188 \times 10^{-2} fs \tag{4.32}$$

We were able to obtain the time duration of the emitted pulses.

CHAPTER 5

RESULT AND DISCUSSION

5.1 Single Colour Lasers

The simulation results due to the interaction of the single colour laser fields with the H atom are presented in this section. Two out of the single colour lasers, been of Ti:Sapphire lasers type were refereed to as fundamental lasers (800 nm), while the other refereed to as the secondary laser (400 nm), is a laser source in the visible region of the EM spectrum.

5.1.1 Case 1 (a): 1^{st} Fundamental Laser Field

The characteristics of the first fundamental field considered is of the 800 nm pulsed Ti:Sapphire laser of 2 $\times 10^{14}$ W/cm^2 intensity, with 10 cycles in a pulse. The results of their interaction with the H atom are presented below;

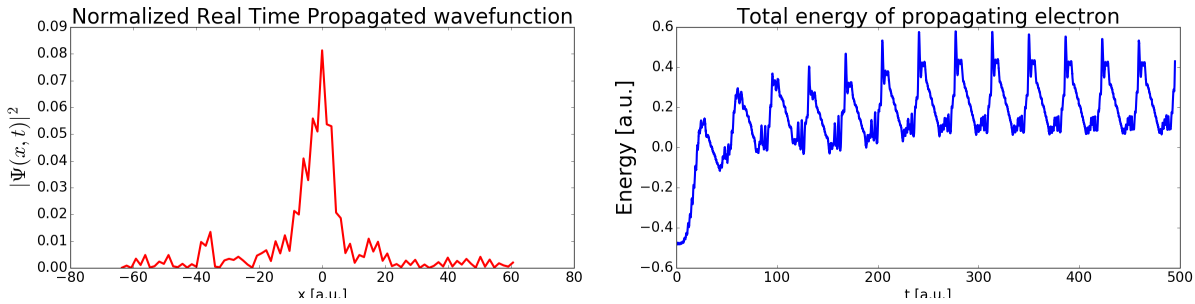

(a) (b)

Figure 5.1: The 1^{st} fundamental electron density and total energy of the propagating electron

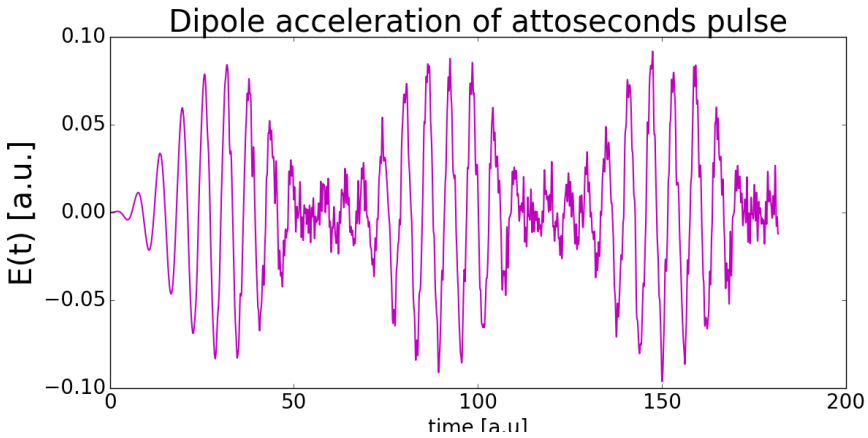

Figure 5.2: 1^{st} fundamental field dipole acceleration

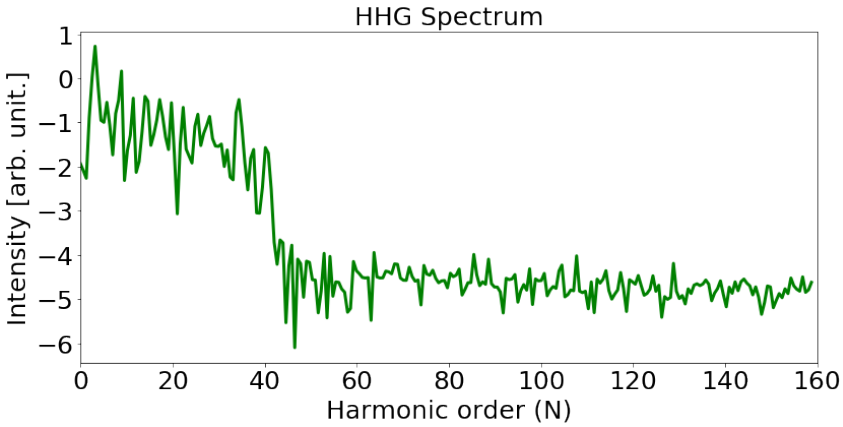

Figure 5.3: 1^{st} fundamental field HHG spectrum

The probability density plot of the evolving electron wavepacket is as shown in Figure 5.1a. The time axis which was not represented in the plot can be visualized as a perpendicular extension of the position grid, pointing inward into the page. The electron travelled away from the soft core, but within -40 to 20 $a.u.$ of position. The above plot is in good agreement with the 2^{nd} postulate of the SFA Model, in that the depletion of the ground state is ignored. i.e. not all of the electron wavepacket leaked out of the core. The percentage of unionised electron density, that remained in the ground state is computed thus;

$$\text{unionised fraction} = 1 - \frac{|\psi|^2_{\text{ground state}} - |\psi|^2_{\text{propagated}}}{|\psi|^2_{\text{ground state}}} \tag{5.1}$$

$$\text{unionised } \% = 1 - \left[\frac{0.1 - 0.083}{0.1} \times 100\right] \tag{5.2}$$

$$= 20.48 \ \% \tag{5.3}$$

So, about 80 % of $|\psi(x,0)|^2$ was leaked out. The total instantaneous total energy of the oscillating electron is as shown in Figure 5.1b. Just before ionization, the electron is restricted to be within the core with a binding energy of -0.5 $a.u.$But upon irradiation with the laser, the electron tunnels out into the continuum with approximately zero energy. The several peaks shows that the electron was on several times ionized and subsequently recombined with the core. The energy of the electron became approximately stable beyond 200 $a.u.$ of time, and by taking the average we measured 0.55 $a.u.$ energy.

$$\therefore E_{\text{total energy}} = 0.55 \ \ a.u. \tag{5.4}$$

We observed that the electron's initial energy corresponds approximately to I_p i.e. the energy contribution from excited bound states had no effect. Thus, the result of the energy plot also follows closely the 1^{st} postulate of the SFA Model in section 2.1.2

The dipole acceleration of the generated pulse is as shown in Figure 5.2. This corresponds to the electric field profile of the attosecond pulse. It's profile shows resemblance with the driving laser field, which means that it depends on the laser field. The attosecond pulse has a periodicity of 55 $a.u.$ of time. From Appendix A we have that;

$$1 \text{ a.u. of time} = 2.4188 \times 10^{-2} \ \ fs \tag{5.5}$$

so that

$$55 \text{ a.u.} = 2.4188 \times 10^{-2} fs \times 55 \tag{5.6}$$

$$\approx 1330 \times 10^{-18} \ s \tag{5.7}$$

$$\approx 1330 \ as \tag{5.8}$$

Eq.5.8 which represents the pulse duration appears to be too large as against 10^2 orders of attoseconds pulse that are currently been generated. The large number of cycles in Figure 5.2 explains the reason for the large pulse duration. The HHG spectrum of the corresponding attosecond pulse is as shown in Figure 5.3. The plateau extends from the 8^{th} to 35^{th} order, after which there was a sharp cut off. By using Eq.5.4, the harmonic order at the cut-off is calculated thus;

$$N = \frac{|I_p| + 3.17E_{\text{total energy}}}{\omega} \tag{5.9}$$

$$N = \frac{0.5 + 3.17(0.55)}{0.057} \tag{5.10}$$

$$N \approx 39.4 \tag{5.11}$$

We thus see that harmonic cut off order closely corresponded to the result in our HHG spectrum in Figure 5.3. By using Eq2.93, we computed the attosecond pulse energy in eV, thus;

$$8 \text{ harmonic order} = 0.057 \times 27.211 \times 8 \tag{5.12}$$

$$\approx 12.4 \ eV \tag{5.13}$$

Similarly;

$$36 \text{ harmonic order} = 0.057 \times 27.211 \times 35 \tag{5.14}$$

$$\approx 54.3 \ eV \tag{5.15}$$

Each peak in the plateau corresponding to an attosecond pulse have equal intensity and phase orientation. This harmonic order corresponds to 12.4 eV - 54.3 eV (soft x-ray region). Though, the form of the plateau in Figure 5.3 indicated that attosecond pulses are emitted, but the pulses aren't short in time duration.

5.1.2 Case 1(b): 2^{nd} Fundamental Laser Fields ($4 \times 10^{14} W/cm^2$)

The following results are those obtained due to irradiation from an 800 nm pulsed Ti:Sapphire laser of 4 $\times 10^{14}$ W/cm^2 intensity, with 10 cycles in a pulse.

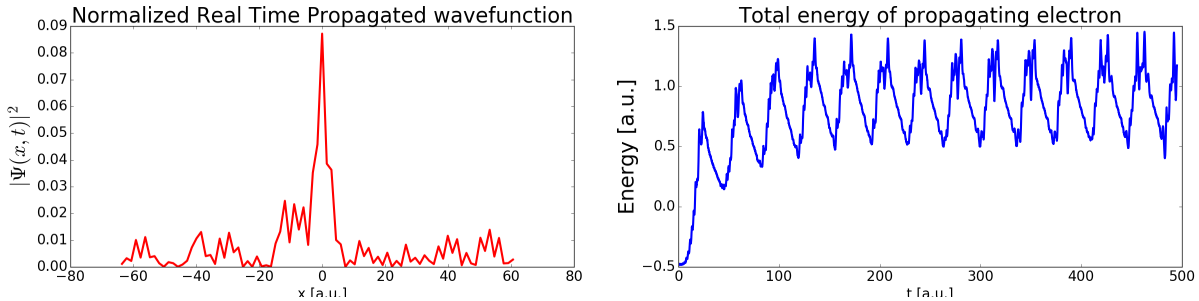

(a) (b)

Figure 5.4: The 2^{nd} fundamental electron density and total energy of the propagating electron.

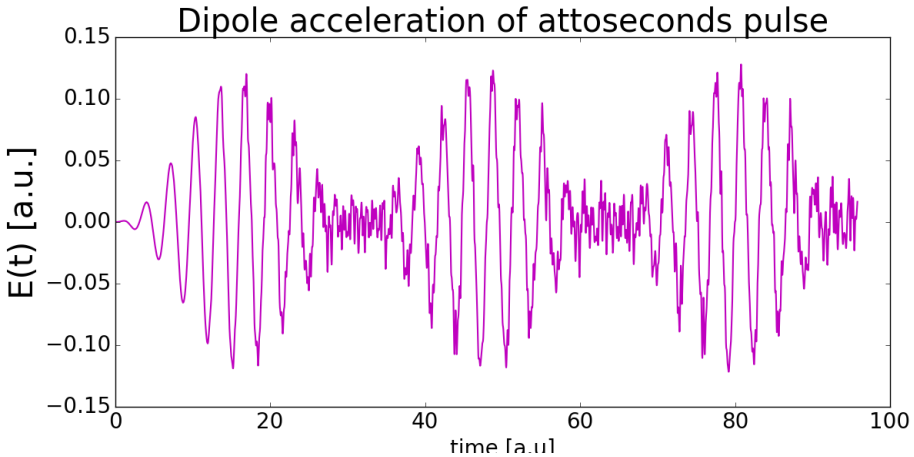

Figure 5.5: 2^{nd} fundamental field dipole acceleration

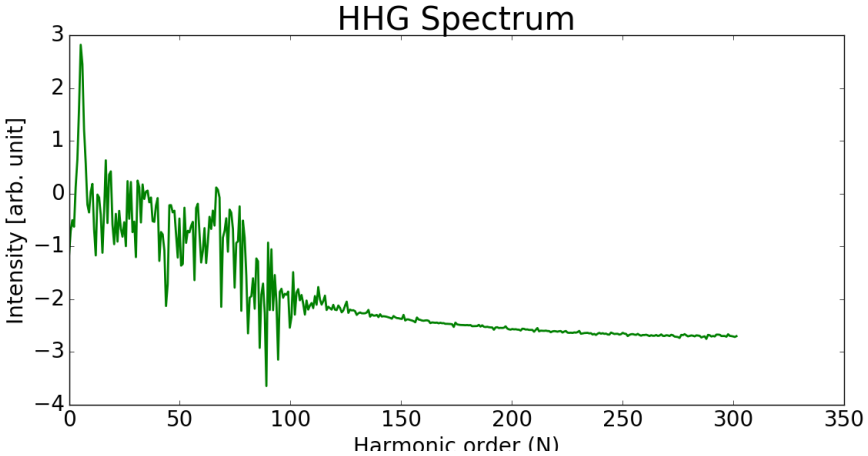

Figure 5.6: 2^{nd} fundamental field HHG spectrum

The probability density of the evolving electron wavepacket is as shown in Figure 5.4a. The electron motion was majorly centered at the origin. We also realized that, the electron

density plot shows that the ground state was not completely depleted. The percentage of unionised electron density, that remained in the ground state is computed using Eq.5.1;

$$\text{unionised } \% = 1 - \left[\frac{0.1 - 0.088}{0.1} \times 100\right] \tag{5.16}$$

$$= 12 \ \% \tag{5.17}$$

We thus see that 88 % of the electron density was leaked out. This again agreed with the SFA assumption. We observed from Figure 5.4b, that when ionization occurred, the electron entered the field with zero energy, and oscillated with an average energy of 1.2 $a.u$, which remained constant beyond 200 $a.u.$ of time. i.e

$$E = 1.2 \ a.u. \tag{5.18}$$

We realized that the electron's initial energy corresponds approximately to I_p, i.e. the energy contribution from excited bound states had no effect. Thus, the result of the energy plot also follow closely the 1^{st} postulate of the SFA Model in section 2.1.2. Figure 5.5 represent the dipole acceleration, whose fourier transforom squared yields the HHG spectrum in 5.6. The attosecond pulse has a periodicity of 28 $a.u.$ of time. From Appendix A we have that;

$$1 \text{ a.u. of time} = 2.4188 \times 10^{-2} \ fs \tag{5.19}$$

so that

$$28 \text{ a.u.} = 2.4188 \times 10^{-2} fs \times 28 \tag{5.20}$$

$$\approx 677 \times 10^{-18} \ s \tag{5.21}$$

$$\approx 677 \ as \tag{5.22}$$

Eq.5.22 which represents the pulse duration is of the order of 10 less than that obtained in case 1(a). The HHG spectrum of the corresponding attoseconds pulse is as shown in Figure 5.6. The plateau extends from 25^{th} to 75^{th} order, after which there was a sharp cut off. By using Eq.5.18, the harmonic order at the cut-off is calculated thus;

$$N = \frac{|I_p| + 3.17E_{\text{total energy}}}{\omega} \tag{5.23}$$

$$N = \frac{0.5 + 3.17(1.2)}{0.057} \tag{5.24}$$

$$N \approx 75.5 \tag{5.25}$$

We thus see that harmonic cut off order closely corresponded to the result in our HHG spectrum in Figure 5.6. By using Eq.2.93, we computed the attoseconds pulse energy in eV, thus;

$$25 \text{ harmonic order} = 0.057 \times 27.211 \times 25 \tag{5.26}$$

$$\approx 38.7 \ eV \tag{5.27}$$

Similarly;

$$75 \text{ harmonic order} = 0.057 \times 27.211 \times 75 \tag{5.28}$$

$$\approx 116.3 \ eV \tag{5.29}$$

Each peak in the plateau corresponding to an attosecond pulse have equal intensity and phase orientation. This harmonic order corresponds to 39 eV - 116 eV (soft x-ray region). Though the form of the plateau in Figure 5.6 indicated that attosecond pulses are emitted but, it would pose great difficulty in isolating a single pulse due to the likely *short pulse repetition* rate of the pulse train.

5.1.3 Case 2 : Secondary Laser Field

The following results are those obtained due to irradiation from a 400 nm pulsed visible laser of 4 $\times 10^{14}$ W/cm^2 intensity, with 20 cycles in a pulse.

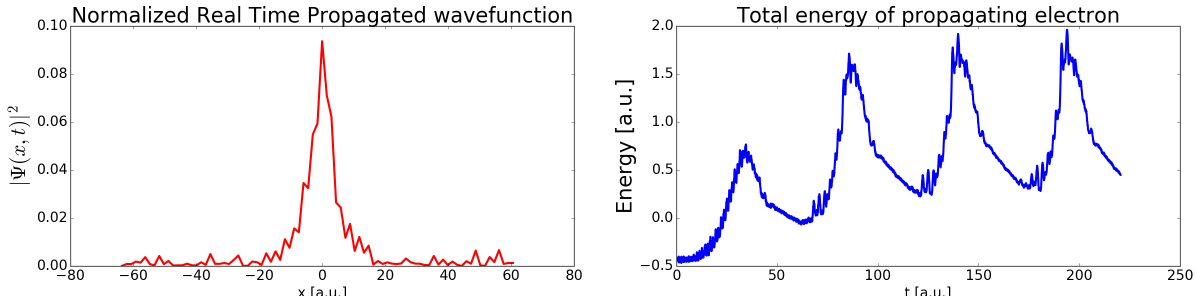

(a) (b)

Figure 5.7: The secondary electron density and total energy of the propagating electron

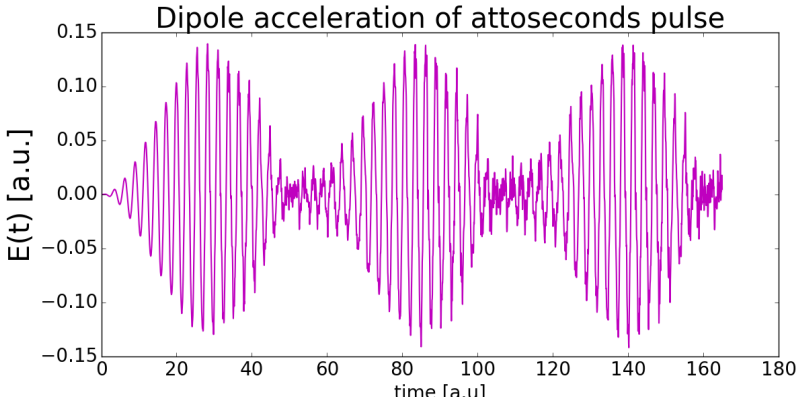

Figure 5.8: The secondary field dipole acceleration

The snapshot of the electron possible position at an instance of time is as shown in Figure 5.7a. As before, the electron underwent ionization, followed by propagation and subsequently recombination.
The percentage of unionised electron density, that remained in the ground state is computed using Eq.5.1;

$$\text{unionised } \% = 1 - \left[\frac{0.1 - 0.095}{0.1} \times 100\right] \tag{5.30}$$

$$= 15 \ \% \tag{5.31}$$

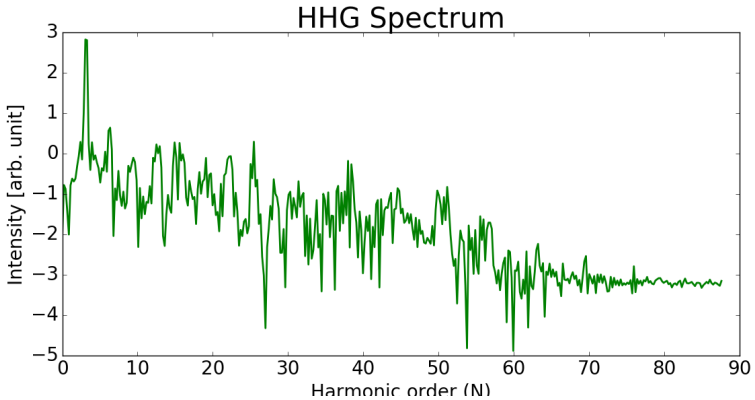

Figure 5.9: The secondary field HHG spectrum

We thus see that 85 % of the electron density was leaked out. This again agreed with the SFA assumption. It is the same result as for case 1(b). The total instantaneous total energy of the oscillating electron is as shown in Figure 5.7b. Just before ionization, the electron is restricted to be within the core with a binding energy of -0.5 $a.u.$, upon irradiation with the laser, the electron tunnels out into the continuum with approximately zero energy. The several peaks shows that the electron was on several times ionized and subsequently recombined with the core. The energy of the electron became approximately stable beyond 100 $a.u.$ of time, and by taking the average, we measured 1.50 $a.u.$ energy. i.e

$$E = 1.70 \ a.u. \tag{5.32}$$

We observed that the electron's initial energy corresponds approximately to I_p, which is an indication that the energy contribution from excited bound states had no effect. Thus, the result of the energy plot also follow closely the 1^{st} postulate of the SFA Model in section 2.1.2

The dipole acceleration plot is as shown in Figure 5.8. It consisted of about 20 cycles just as the same number of cycles in the driving laser field. The attosecond pulse has a periodicity of about 50 $a.u.$ of time. From Appendix A we have that;

$$1 \text{ a.u. of time} = 2.4188 \times 10^{-2} \ fs \tag{5.33}$$

so that

$$50 \text{ a.u.} = 2.4188 \times 10^{-2} fs \times 50 \tag{5.34}$$

$$\approx 1379 \times 10^{-18} \ s \tag{5.35}$$

$$\approx 1209 \ as \tag{5.36}$$

Eq.5.36 which represents the pulse duration appears to be too large owing to the large number of cycles in the dipole acceleration. The HHG spectrum of the corresponding attoseconds pulse is as shown in Figure 5.9. Two plateau peaks were observed, the first extended from 5^{th} to 25^{th} order, while the other extended from 28^{th} to 50^{th} order after which there was a sharp cut off. The cut-off in the second plateau approximately corresponded to the cut off corresponding to Figure 5.7b. The harmonic order at the cut-off is calculated thus;

$$N = \frac{|I_p| + 3.17E_{\text{total energy}}}{\omega} \tag{5.37}$$

$$N = \frac{0.5 + 3.17(1.7)}{0.113886} \tag{5.38}$$

$$N \approx 51.7 \tag{5.39}$$

We thus see that, the harmonic cut off order approximately corresponded to the result in our HHG spectrum in Figure 5.9. By using Eq.2.93, we computed the attosecond pulse energy in eV as per;

$$50 \text{ harmonic order} = 0.113886 \times 27.211 \times 50 \tag{5.40}$$

$$\approx 154.9 \ eV \tag{5.41}$$

Similarly

$$28 \text{ harmonic order} = 0.113886 \times 27.211 \times 28 \tag{5.42}$$

$$\approx 86.77 \ eV \tag{5.43}$$

Each peak in the plateau corresponding to an attoseconds pulse have equal intensity and phase orientation. This harmonic order corresponds to 87 eV - 155 eV (soft x-ray region). Though the form of the plateau in Figure 5.9 indicated that attosecond pulses are emitted but, it would some difficulty in filtering out a single pulse from the the trains of pulses following from our discussion in Chapter 3.

5.2 Two Colour Mixing

The interaction between the 1^{st} fundamental and secondary laser field gave rise to the two colour mixing, whose resultant field is referred to as the synthesized field. Here we considered the effect of introducing the secondary laser source to jointly interact also with the H atom, and by excluding and/or including a time delay, we realized an improvement in the results over irradiation by a single coloured beam. A larger grid size was used in the computation for the two colour mixing.

5.2.1 Two Colour without Time Delay

In the form of the synthesized laser field as given by Eq.4.20, by setting τ to be zero, we have obtained marked differences in our results, whose respective plots are shown below. The plot in Figure 5.10a revealed that the electron was at the origin at some point in time, while at other time it was propagating along the left and right sides of the grid. Due to the absorber, the electron motion was restricted from approaching the grid edges.

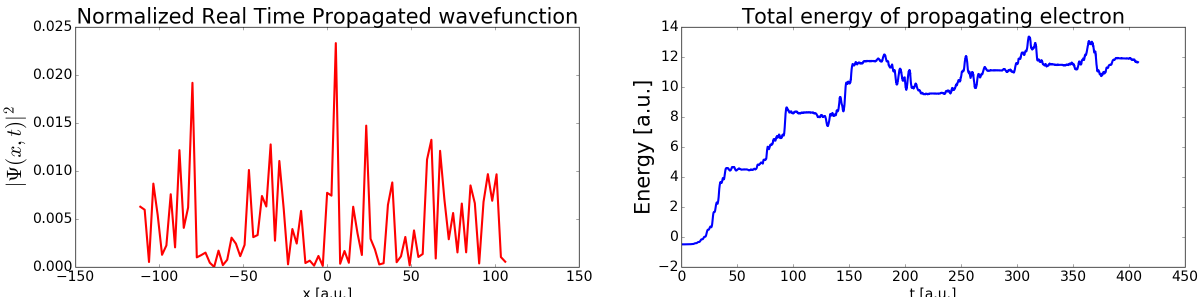

(a) (b)

Figure 5.10: 1^{st} Two color electron density and total energy plot

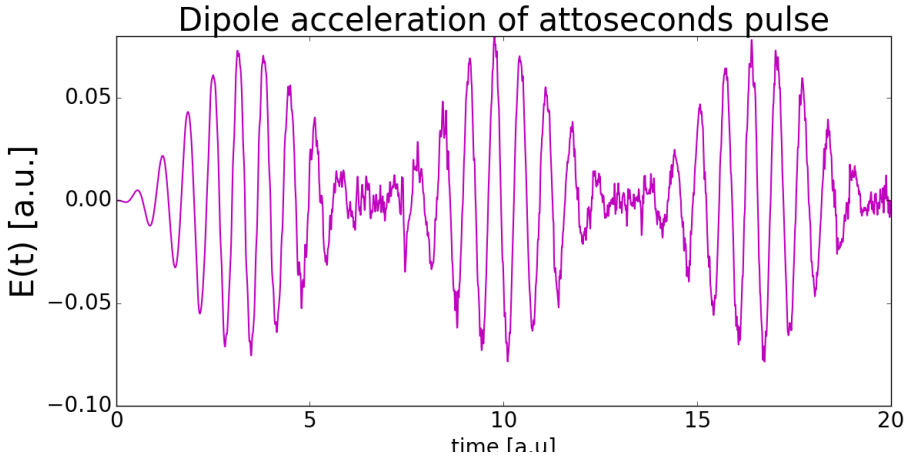

Figure 5.11: 1^{st} Two color dipole acceleration.

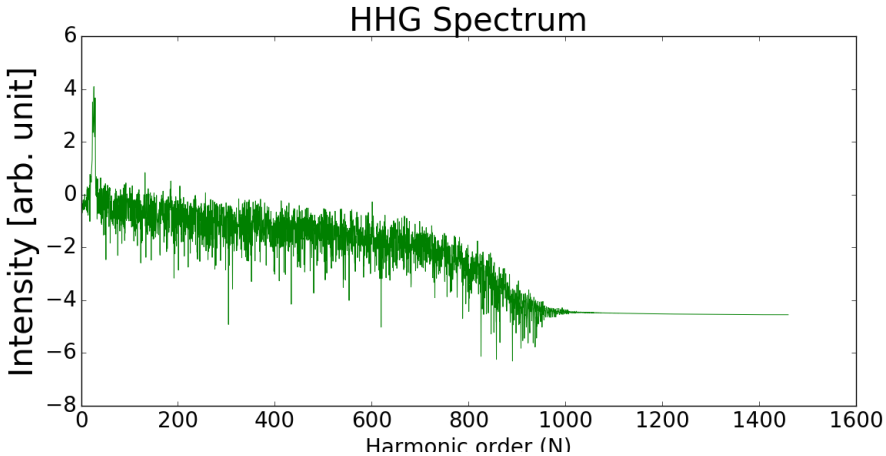

Figure 5.12: 1^{st} Two color HHG spectrum

By using Eq.5.1 we found out that 23 % of the electron density remained in the ground state, during propagation. The total energy gained by the electron is as shown in Figure 5.10b. The electron ionizes and gains energy progressively until its energy become stabilized at around 22 - 48 $a.u.$ of time. The stabilized energy is about 12 $a.u.$ energy. The attosecond pulse has a periodicity of 7.00 $a.u.$ of time. From Appendix A we have that;

$$1\text{a.u. of time} = 2.4188 \times 10^{-2}\ fs \tag{5.44}$$

so that

$$0.65 \text{ a.u.} = 2.4188 \times 10^{-2} fs \times 7.00 \tag{5.45}$$

$$\approx 169.3 \times 10^{-18} \ s \tag{5.46}$$

$$\approx 169 \ as \tag{5.47}$$

Eq.5.47 which represents the pulse duration is of the order of 10^2. The dipole acceleration of the corresponding attosecond pulse is as shown in Figure 5.11, consisting of three pulses. It mimics the electric field profile of the generated attosecond pulses. Hence we observed that the pulses have been emitted coherently. It shows some marked differences compared to that of the single color. The attosecond pulses emitted , were of very short duration. It appeared that the shorter the pulses, the less intense the field would appear to be [1]. It tuns out that *attosecond pulses (in Figure 5.11) were less intense than the pulses produced in Figures 5.5 and 5.8.* From our discussion in Chapter 3, we know that, a very short attosecond pulse generation is an indication of a broad plateau. This made the plateau to appear broad as seen in Figure 5.12 extending from 200^{th} - 673^{th} order. The harmonic order at the cut-off is calculated as per;

$$N = \frac{|I_p| + 3.17 E_{\text{total energy}}}{\omega} \tag{5.48}$$

$$N = \frac{0.5 + 3.17(12.0)}{0.057} \tag{5.49}$$

$$N \approx 676 \tag{5.50}$$

We thus see that the harmonic cut off order corresponded closely to the result in our HHG spectrum in Figure 5.12. By using Eq.2.93, we computed the attosecond pulse energy in eV, as per;

$$200 \text{ harmonic order} = 0.057 \times 27.211 \times 200 \tag{5.51}$$

$$\approx 310.2 \ eV \tag{5.52}$$

Similarly;

$$673 \text{ harmonic order} = 0.057 \times 27.211 \times 673 \tag{5.53}$$

$$\approx 1043.84 \ eV \tag{5.54}$$

Each peak in the plateau corresponding to an attosecond pulse have equal intensity and phase orientation. The harmonic order corresponds to 310 eV - 1044 eV (hard x-ray). The broad plateau region forming the continuum length indicated that an isolated attosecond pulse is realizable.

[1] High energy attosecond pulses usually have lower intensity and vice versa

5.2.2 Two Colours With Time Delay

The time delay consideration is for the case where $\tau \neq 0$. As an important note, the fundamental laser has a pulse duration T_p, of about 3536 $a.u.$ of time (refer to Appendix A), which also happen to be secondary laser pulse duration. For a given phase ϕ, we computed the corresponding time delay τ as a fraction of this period, by using Eq.3.6.

(i) **Consideration for phase, $\phi = 0.04\pi$**

$$\tau = \frac{\phi}{\omega} \tag{5.55}$$

where $\omega = \frac{2\pi c}{\lambda}$, $\omega_1 = \frac{2\pi c}{\lambda_1}$, λ is the wavelength of the fundamental laser field, λ_1 is the wavelength of the secondary laser field, τ is the time lag. $\lambda = 800\ nm$, $\lambda_1 = 400\ nm$. By converting into atomic unit (See Appendix A). We have

$$\tau = \frac{0.04 \times 1768}{0.057} \approx 50\ a.u \tag{5.56}$$

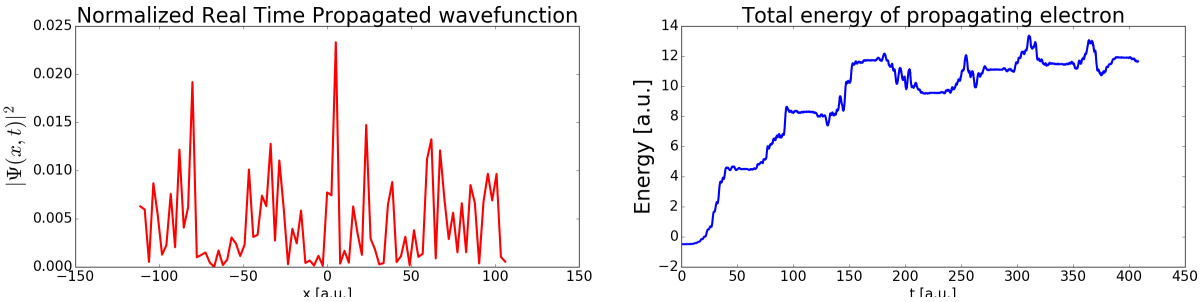

(a) (b)

Figure 5.13: 2^{nd} two colour electron density and total energy plot

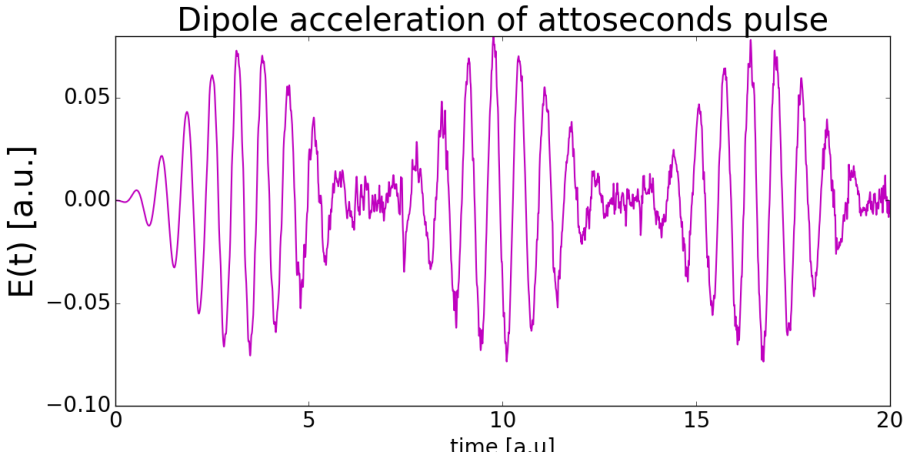

Figure 5.14: 2^{nd} two colour dipole acceleration

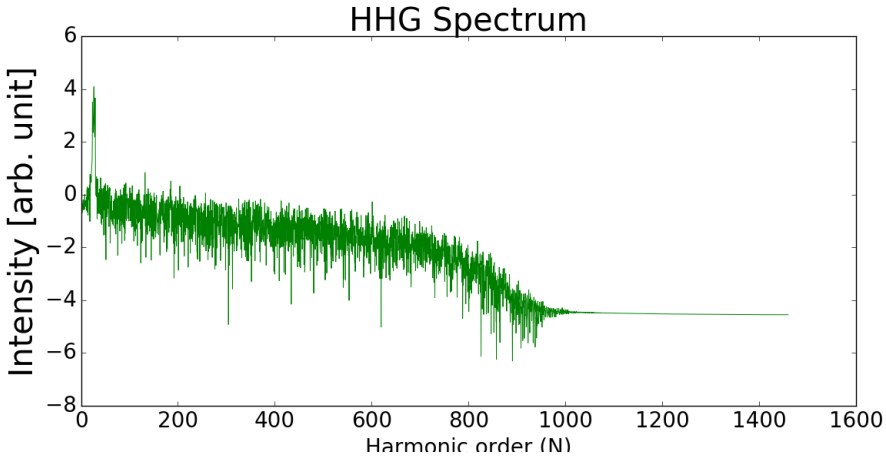

Figure 5.15: 2^{nd} two colour HHG spectrum

(ii) **Consideration for phase, $\phi = 0.2\pi$**

Using Eq.5.55 it follows that;

$$\tau = \frac{0.2 \times 1768}{0.057} \approx 400 \ a.u$$

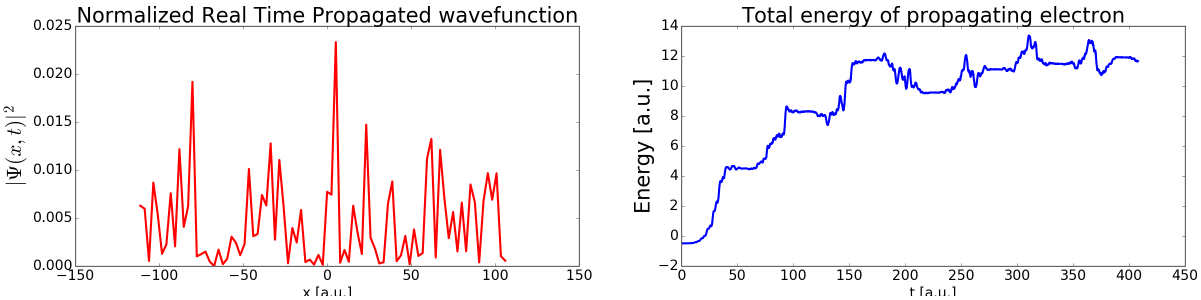

(a) (b)

Figure 5.16: 3^{rd} two color electron density and total energy plot

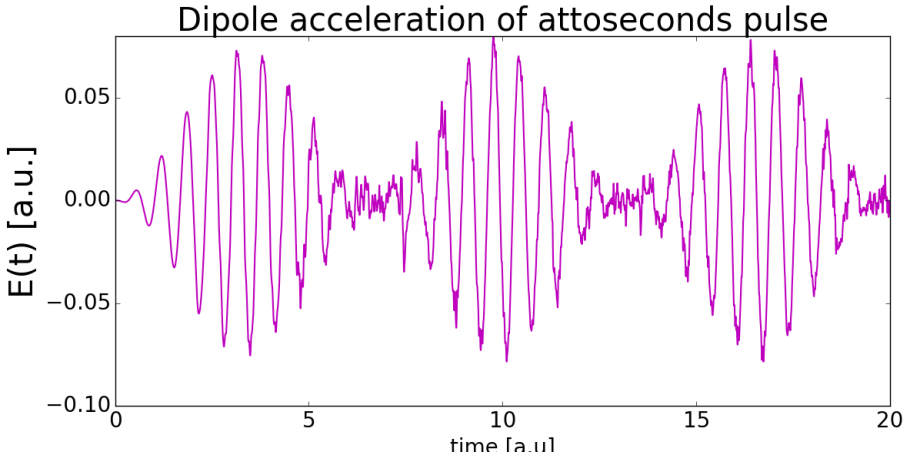

Figure 5.17: 3^{rd} two colour dipole acceleration

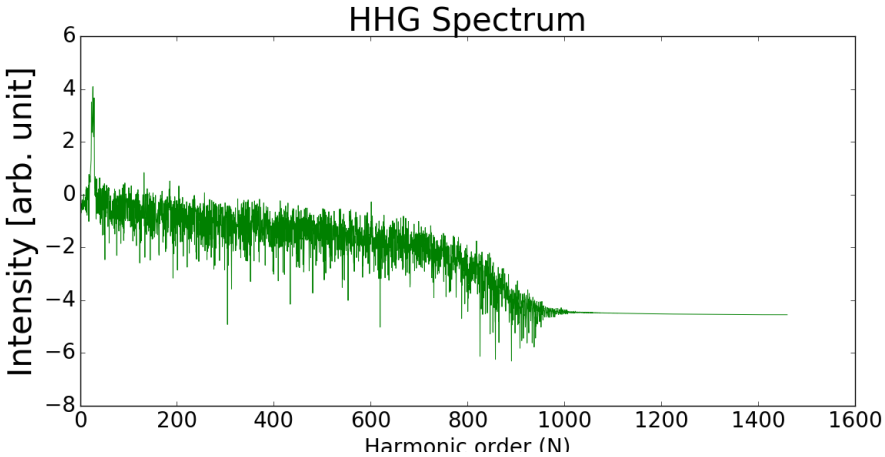

Figure 5.18: 3^{rd} two colour HHG spectrum

(iii) **Consideration for phase,** $\phi = \pi$

Using Eq.5.55, it follows that;

$$\tau = \frac{1768}{0.057} \approx 1768 \ a.u$$

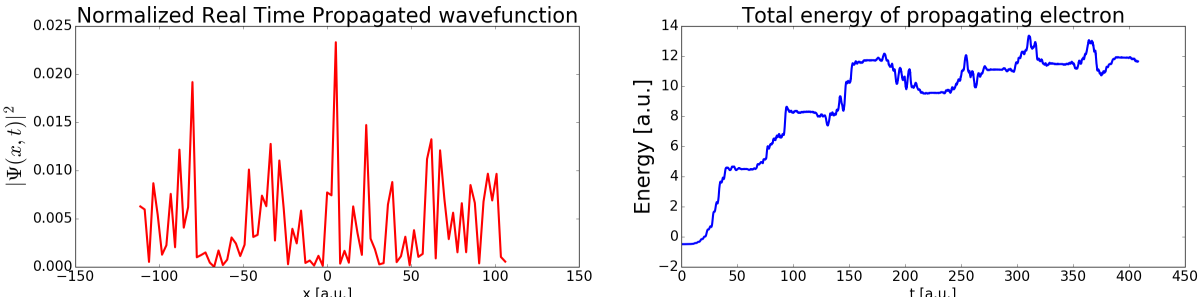

(a) (b)

Figure 5.19: 4^{th} two color electron density and total energy plot

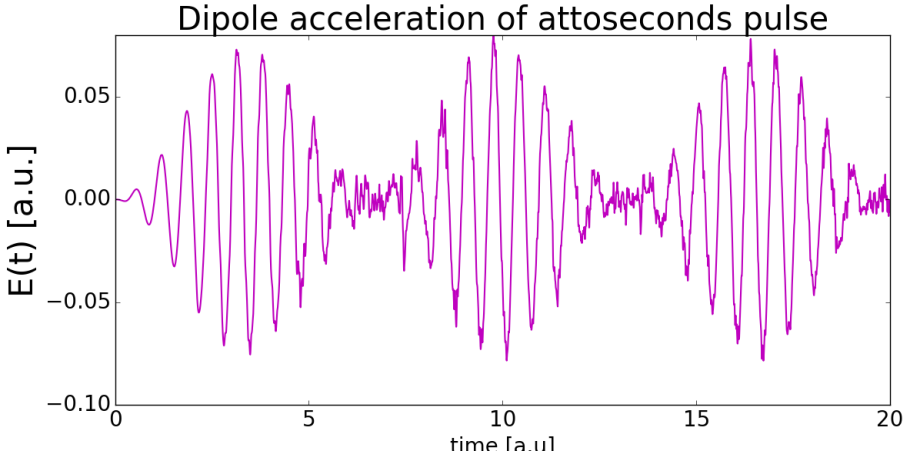

Figure 5.20: 4^{th} two color dipole acceleration

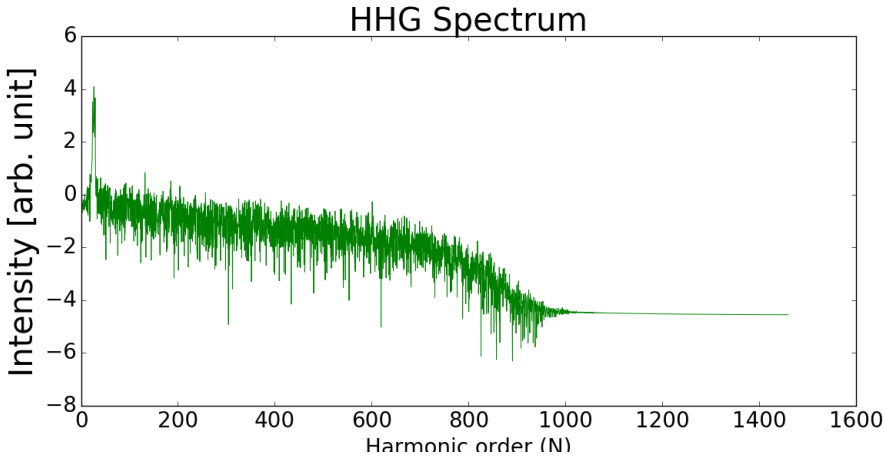

Figure 5.21: 4^{th} two color HHG spectrum

(iv) **Consideration for phase, $\phi = 1.6\pi$** Using Eq.5.55, it follows that;

$$\tau = \frac{1.6 \times 1768}{0.057} \approx 3203 \ a.u$$

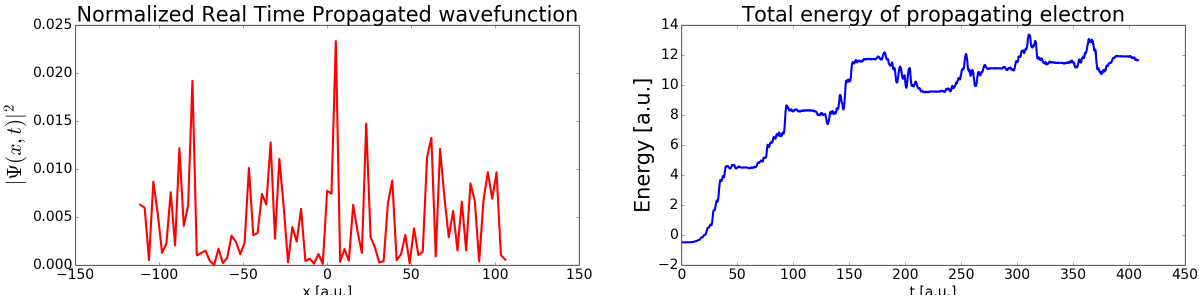

(a) (b)

Figure 5.22: 5^{th} two color electron density and total energy plot

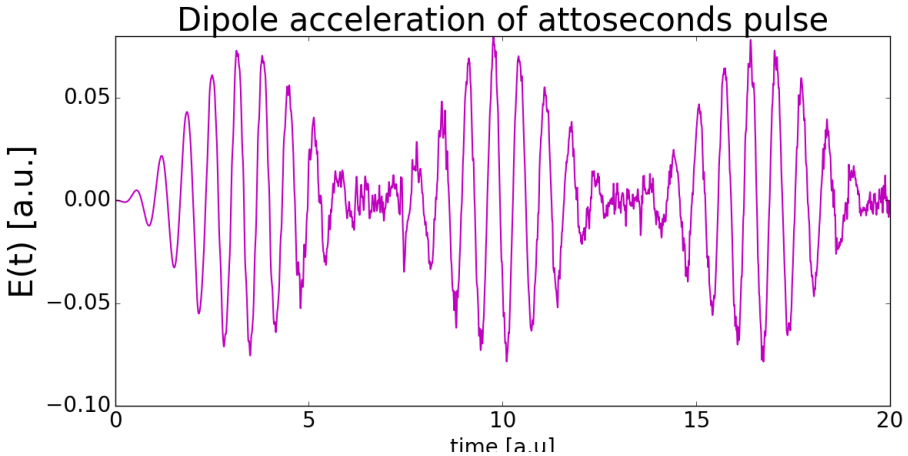

Figure 5.23: 5^{th} two color dipole acceleration

We observed that all the results for time lag consideration appeared exactly the same as those obtained in 5.10, 5.11 and 5.12. So, we conclude that the system was already optimized for the initially chosen laser parameters.

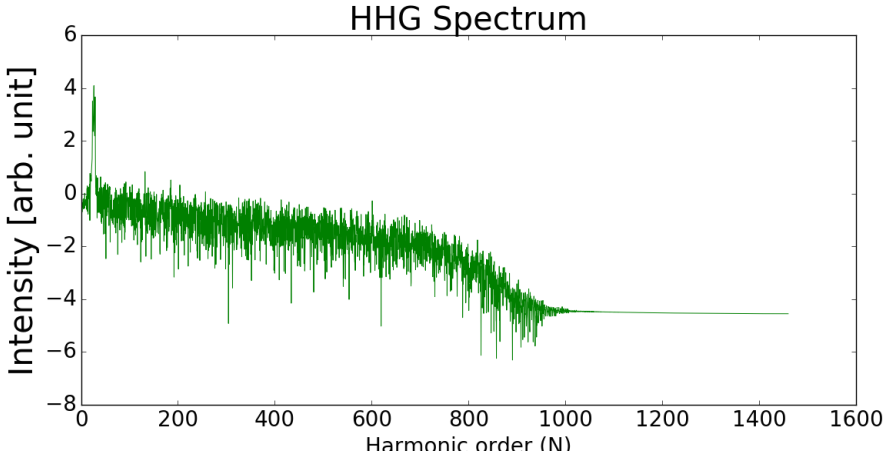

Figure 5.24: 5^{th} two color HHG spectrum

CONCLUSION

The aim of this research was to study the response of an H atom in the presence of a moderately intense laser field, with respect to generating trains of attosecond pulses and single attosecond pulse. We started by reviewing the basic fundamentals of femtosecond lasers needed for a proper comprehension of the HHG process attributed to attosecond production. Subsequently, we considered the production mechanism of femtosecond lasers, unique properties as a *super light* and their mathematical representation were examined too.

The HHG process that produces a multiplier effect of the incident femtoseconds laser energy upon laising with an atomic system was well understood via the Simple-man's Model, Lewestein Model and direct TDSE simulation Model. However, owing to the observed low conversion efficiency of the simplified HHG process, and the need to generate a single attosecond pulse, the two-color scheme was strongly reviewed, been the common theoretical technique for generating an ultrashort single pulse whose energy extends into the X-ray regime.

Our particular interest was on pushing the cut-off energy limit farther into the EM spectrum scale (into the extreme ultraviolet- hard X ray region). In the theory of our work, we derived the 1D non-relativistic Schrodinger equation for an H atom using the dipole approximation and whose solution was obtained by the split operator method. In our computer work, the resultant wavefunction was simulated and propagated in momentum (p) and space (x) configuration by Fast Fourier Transforming back and forth between p and x, and finally expressed in x configuration.

For the case of the imaginary time propagation (where the H system was back propagated in time to relax it to its ground state), the resulting ground state wavefunction was used to compute the ground state energy. This ground state wavefunction served as the initial wavefunction in the real time propagation. The energy profile of the laser-driven electron showed that ionization, propagation and recombination occurred multiple times resulting to the generation of trains of pulses. The final wavefunction from the real time propagation was used to compute the HHG spectrum of the generated harmonics. And by computing the electric field profile describing the generated attosecond pulse, the time profile indicating the pulse duration was calculated.

We have employed different characteristics laser forms. For the three forms of the single-coloured laser used, the real time propagated electron wavepacket, energy profile, pulse electric profile plot and HHG spectrum was computed. When the fundamental Ti:Sapphire laser with the parameters 800 nm, $2{\times}10^{14} W/cm^2$, 10 cycles irradiated the H atom, a train of 1330 as pulses extending from the 8^{th} - 36^{th} harmonic order corresponding to 12 eV -55.8 eV was generated. When another fundamental Ti:Sapphire laser with the parameters 800 nm, $4{\times}10^{14} W/cm^2$, 10 cycles irradiated the H atom, a train of 677 as pulses extending from the 25^{th} - 75^{th} harmonic order corresponding to 39 eV - 116 eV was generated. Furthermore, by when a secondary laser source in the far visible region with the parameters 400 nm, $5{\times}10^{14} W/cm^2$, 20 cycles irradiated the H atom, we obtained a train of 1209 as pulses extending from the 28^{th} - 50^{th} harmonic order corresponding to 87 eV

- 155 eV.

In a bid to extend the spectral cut-off energy, we generated a synthesized laser from the interference of the fundamental and secondary laser. Upon the introduction of the synthesized laser, a broad plateau region occurred corresponding to a single attosecond been generated. As a means of trying to optimize our result, several time delay were introduced into the system by varying the Carrier Envelope Phase, ϕ. We however noticed that the corresponding results were similar to those obtained without time delay. In both cases, an isolated 169 as pulse was observed having a maximum of 685 harmonic order corresponding to 1.044 keV of energy. This is an incredible result which can be achieved experimentally owing to the recent experimental generation of the driving pulsed laser used in the simulation.

APPENDIX A

ATOMIC UNIT CONVERSION

$m = \hbar = e = 1$
1 $a.u.$ of time $= 2.4188 \times 10^{-2} fs$
1 $a.u.$ of position $= 5.29177 \times 10^{-2} nm$
1 $a.u.$ of velocity $= 2.188 \times 10^{6} m/s$
1 $a.u.$ of frequency $= 4.1341 \times 10^{16} s^{-1}$
1 $a.u.$ of permitivity $= 4\pi \times 8.8542 \times 10^{-2} As/Vm$
1 $a.u.$ of energy $= 4.3597 \times 10^{-18} J = 27.211 eV$

This code was written in Python programming language, It was compiled on an unbuntu system with IP[y]:Notebook (Python version: Python 3.5.2)

```
### DOUBLE COLOR (synthesized field)###

### Parameters of fundamental laser ###
E0=np.sqrt(2e14/3.51e16) # amplitude of the driving laser
w =0.057# angular frequency of the driving laser
T =2 *np.pi/w # time duration of a single cycle in the driving laser
nc =  10


### Parameters of secondary laser ###
E01=np.sqrt(5e14 /3.51e16) # amplitude of the driving laser
w1 = 0.113886143 # angular frequency of the driving laser
T1 =2 *np.pi/w1 # time duration of a single cycle in the driving laser
nc1 = 20


############ Time delay variation ##################
tau_d = 0.0
#tau_d = 50.0
#tau_d = 400.4 # corresponds to (0.2 * pi)/w
#tau_d = 17684.3 # corresponds to pi/w
#tau_d = 3203.2 # corresponds to (1.6 * pi)/w

##### parameters for IMAGINARY TIME PROPAGATION ####
TM = 85 #temporal grid size
dp_im =  0.03767209
ic= complex(0,1) #imaginary quantity, sqrt(-1)
dt_im=-ic*dp_im #time step
```

```
p_im = 0.0 #initial time
### parameters for  REAL TIME PROPAGATION ####
GG_r = 8000 #temporal grid size
dt_r =5.10006600e-02 #time step
p_r = 0.0 #initial time
######## parameters for COMPUTING THE HHG SPECTRUM #######
GG_sp = GG_r #temporal grid size
dt_sp =0.6006600e-02
p_sp = 0 #initial time



a = 0.4582 # the soft core parameter
Nx = TM # no of points in the position grid
Lx =7.0 # lenght of the position grid

### points in the position grid ###
x = [i*10.0*np.pi*(Lx/Nx) for i in range(-Nx /2, 1+Nx/2)]
### points in the momentum grid ###
k_x = (1.0/Lx)*np.array([ic*n for n \
                         in range(0,Nx/2) + [0] + range(-Nx/2+1 ,0)])

Xmin=min(x) # minimum point in the position grid
Xmax=max(x) # maximum point in the position grid
dx =(Xmax-Xmin)/Nx # time step in the position grid

x1 = Xmax-(5.*np.pi*Lx)/10.0 # RHS location of the absorber pot.
x2 = Xmin +(5.*np.pi*Lx)/10.0 # LHS location of the absorber pot.

###initiatilization of the momentum,position,soft core parameter###
k2xm=np.zeros(Nx, dtype=float)
xx=np.zeros(Nx, dtype=float)
av=np.zeros(Nx, dtype=float)

for i in range(Nx):
    k2xm[i] = abs(np.real(k_x[i]**2)) # momentum squared
    xx[i]=x[i]
    av[i]=a

### soft core potential ###
Vs= - 1/(np.sqrt(xx**2 + a**2))


### initialization of  other parameters ###
pot=np.zeros(Nx, dtype= float)
pott=np.zeros(Nx, dtype= float)
u=np.zeros(Nx, dtype= complex)
una=np.zeros(Nx, dtype= complex)
unb=np.zeros(Nx, dtype= complex)
v=np.zeros(Nx, dtype= complex)
```

```
vna=np.zeros(Nx, dtype= complex)
vnb=np.zeros(Nx, dtype= complex)
Vopt = np.zeros(Nx, dtype= complex)

### Initial wavefunction ####
alpha =1.0
uinit =np.exp((-alpha*xx**2)/2) # initial wavefuntion
usinit =abs(uinit)** 2
I_usinit = usinit
norm2i =0
for i in range(Nx):
    norm2i += usinit[i]*dx
u= uinit/(norm2i**0.5)#normalized initial wavefuntion
I_u = u


#### Laser PotentialS #######
def Vlaserp(xx ,pp,E0): # potential of fundamental lasers
    vv = -xx*E0*np.sin(w*pp)*(np.sin((np.pi*pp)/(T*nc)))** 2
    return vv
def Vlaserp1(xx ,pp,E01): # potential of secondary lasers
    vv1 = -xx*E01*np.sin(w1*(pp + tau_d))*(np.sin(((np.pi*pp)/(T1*nc1))+tau_d))**2
    return vv1


#### Absober Potential ######
def thetax(yy): #theta = absorption strength
    if yy > 0.0 :
        return 0.5
    else:
        return 0.0

for i in range(0,Nx):
    Vopt[i] = (thetax(xx[i]-x1)*((xx[i]-x1)/(Xmax-x1))**2 \
         + thetax(x2-xx[i])*((xx[i]-x2)/(Xmin-x2))**2)


       ### IMAGINARY TIME PROPAGATION ###

       ### REAL TIME PROPAGATION ###

       ### COMPUTING THE HHG SPECTRUM ###

                ### PLOTS ###
```

BIBLIOGRAPHY

[1] Aleksander Skjerlie Simonsen, Tor Kjellsson, Morten Førre, Eva Lindroth, and Sølve Selstø; *Ionization dynamics beyond the dipole approximation induced by the pulse envelope*, Physical Review 93, 053411(2016).

[2] Kenichi L. Ishikawa ; *Chapter 19, High Harmonic Generation, Advances in Solid State Lasers Development and Applications*, Mikhail Grishin (Ed.), ISBN: 978-953-7619-80-0, 2010

[3] Gao Chen and Feng-Dong Zhang ; *Analysis of Isolated Attosecond Pulse Generation from a Multi-cycle Two-color Pulse*, Journal of the Korean Physical Society, Vol. 62, No. 1, January 2013, pp. 34-39

[4] T. Nemati Aram, S. Batebi, and M. Mohebbi; *Numerical Simulation of an Intense Isolated Attosecond Pulse by a Chirped Two-Color Laser Field*, International Journal of Optics and Photonics (IJOP), Vol. 6, No. 1, Winter-Spring, 2012

[5] Byunghoon Kim, Jungkwen Ahn, Yongli Yu, Ya Cheng, Zhizhan Xu, and Dong Eon Kim,; *Optimization of multi-cycle two-color laser fields for the generation of an isolated attosecond pulse*, 7 July 2008, Vol.16, No.14 Optics Express 10333

[6] Yongli Yu1, Xiaohong Song, Yuxi Fu1, Ruxin Li1, Ya Cheng, and Zhizhan Xu1; *Theoretical investigation of single attosecond pulse generation in an orthogonally polarized two-color laser field* , 21 January 2008, Vol. 16, No.2 Optics Express 686.

[7] Dian Peng, Liang-Wen Pi, M. V. Frolov and Anthony F. Starace1; *Enhancing high-order-harmonic generation by time delays between two-color, few-cycle pulses*, Physical Review A 95, 033413 (2017)

[8] M. Lewenstein, Ph. Balcou, M. Yu. Ivanov, Anne L'Huillier, and P. B. Corkum; *Theory of high-harmonic generation by low-frequency laser fields*, Physical Review A Volume 49, Number 3 March 1994

[9] Dejan B. Milosevic, Wilhelm Becker, and Richard Kopold; *Generation of circularly polarized high-order harmonics by two-color coplanar field mixing*, Physical Review A Volume 45, Number 7 May 2000.

[10] Hung-Tzu Chang, Michael Zurch, Peter M. Kraus,1 Lauren J. Borja Daniel M. Neumark and Stephen R. Leone; *Simultaneous generation of sub-5-femtosecond 400 nm and 800 nm pulses for attosecond extreme ultraviolet pump–probe spectroscopy* ,Optics Letter, Vol 41, N0. 22/November 15 2016/Optics Letter

[11] Anatole Habib Kenfack ; *Introduction to Laser-Matter Interaction Lecture notes*, African University of Science and Technology [AUST], Nigeria, 2018.

[12] Ariel Gordon, Robin Santra, and Franz X. Kärtner1; *Role of the Coulomb singularity in high-order harmonic generation*, Physical Review A 72, 063411(2005).

[13] Torsten Leitner; *High order Harmonic Generation as a Possible Seed Source for the Bessey Free Electron Laser,* PhD Thesis submitted to Humboldt-Universitat zu Berlin on 13. August 2007

[14] Emeric Balogh ; *Macroscopic study and control of high-order harmonic and attosecond pulse generation in noble gases*, PhD thesis submitted to the University of Szeged, Physics Doctoral School, 2014.

[15] Frank Grossmann ; *Theoretical Femtoseconds Physics, Atoms and Moecules in Strong Fields*, Springer Series on Atomic, Optical, and Plasma Physics, ISSN 1615-5653, May 2008.

[16] Anh-Thu Le, Hui Wei1, Cheng Jin and C D Lin1; *Strong-field approximation and its extension for high-order harmonic generation with mid-infrared lasers*, J. Phys. B: At. Mol. Opt. Phys. 49 (2016) 053001 (37pp).

[17] Benjamin R. Galloway; *High-Order Harmonic Generation Driven by Mid-Infrared Laser Light*, PhD thesis submitted to the Faculty of the Graduate School of the University of Colorado, 2017.

[18] Mark Csele; *Fundamentals of Light Sources and Lasers*, ISBN 0-471-47660-9, 2004, Published by John Wiley and Sons, Inc., Hoboken, New Jersey

[19] Linda Young1, Kiyoshi Ueda, Markus Gühr, Philip H Bucksbaum, Marc Simon, Shaul Mukame, Nina Rohringer, Kevin C Prince , Claudio Masciovecchio, Michael Meyer, Artem Rudenko, Daniel Rolles, Christoph Bostedt, Matthias Fuchs, David A Reis, Robin Santra, Henry Kapteyn, Margaret Murnane Heide Ibrahim , François Légaré, Marc Vrakking , Marcus Isinger, David Kroon, Mathieu Gisselbrecht, Anne L'Huillier, Hans Jakob Wörner and Stephen R Leone ; *Roadmap of ultrafast x-ray atomic and molecular physics*, J. Phys. B: At. Mol. Opt. Phys. 51 032003, January 2018.

[20] X Y Lai, Qing-Yu Cai and M S Zhan1; *From a quantum to a classical description of intense laser–atom physics with Bohmian trajectories*, New Journal of Physics 11 (2009) 113035 (10pp).

[21] Francesca Calegari, Giuseppe Sansone, Salvatore Stagira, Caterina Vozzi1 and Mauro Nisoli; *Advances in attosecond science*,J. Phys. B: At. Mol. Opt. Phys. 49 (2016) 062001 (27pp).

[22] Ferenc Krausz, Misha Ivanov; *Attosecond physics*,Review of Modern Physics, Volume 81, January-March 2009

[23] Anne-Lise Viotti ; *Efficient generation and characterization of soft x-ray by laser-driven high-order harmonic generation*, Master's thesis at Paul Scherrer Institute (PSI)I, SSN 0280-316X, 2014.

[24] M. D. Feit, J. A. Fleck, JR., and A. Steiger ; *Solution of the Schrödinger Equation by a Spectral Method*, Journal OF Computational Physics 47, 412-433 (1982).

[25] Pascal Diougue Ndione ; *Ultrafast lasers interacting with Small Atoms*, Research essay at African Institute for Mathematical Science (AIMS), 2016.